

ARTICLE

BACH2 drives quiescence and maintenance of resting Treg cells to promote homeostasis and cancer immunosuppression

Francis M. Grant^{1*}, Jie Yang^{1,2*}, Rabab Nasrallah¹, James Clarke^{3,4}, Firas Sadiyah^{1,2}, Sarah K. Whiteside^{1,2}, Charlotte J. Imianowski^{1,2}, Paula Kuo^{1,2}, Panagiota Vardaka^{1,2}, Tihomir Todorov¹, Nordin Zandhuis¹, Ilinca Patrascan^{1,2}, David F. Tough⁵, Kohei Kometani^{7,8}, Robert Eil⁶, Tomohiro Kurosaki^{7,8}, Klaus Okkenhaug², and Rahul Roychoudhuri^{1,2}

Regulatory T (Treg) cell populations are composed of functionally quiescent resting Treg (rTreg) cells which differentiate into activated Treg (aTreg) cells upon antigen stimulation. How rTreg cells remain quiescent despite chronic exposure to cognate self- and foreign antigens is unclear. The transcription factor BACH2 is critical for early Treg lineage specification, but its function following lineage commitment is unresolved. Here, we show that BACH2 is repurposed following Treg lineage commitment and promotes the quiescence and long-term maintenance of rTreg cells. *Bach2* is highly expressed in rTreg cells but is down-regulated in aTreg cells and during inflammation. In rTreg cells, BACH2 binds to enhancers of genes involved in aTreg differentiation and represses their TCR-driven induction by competing with AP-1 factors for DNA binding. This function promotes rTreg cell quiescence and long-term maintenance and is required for immune homeostasis and durable immunosuppression in cancer. Thus, BACH2 supports a “division of labor” between quiescent rTreg cells and their activated progeny in Treg maintenance and function, respectively.

Downloaded from https://rupress.org/jem/article-pdf/217/9/e20190711/1045351/jem_20190711.pdf by guest on 29 June 2020

Introduction

Regulatory T (Treg) cells, characterized by expression of the transcription factor (TF) forkhead box P3 (Foxp3), maintain immune homeostasis by limiting immune reactions directed against self- and innocuous foreign antigens (Benoist and Mathis, 2012; Josefowicz et al., 2012a; Sakaguchi et al., 2008). Two ontogenically distinct subsets of Treg cells are found in peripheral tissues. Thymic Treg (tTreg) cells largely arise from CD4 single-positive (CD4SP) thymocytes in the thymus and are reactive against self-antigens. Peripheral Treg (pTreg) cells arise from naive CD4⁺ T cells in peripheral tissues and are reactive against innocuous foreign antigens often encountered at mucosal sites (Josefowicz et al., 2012b). Treg cell populations exhibit remarkable stability, and their maintenance throughout life is required to prevent lethal inflammation (Kim et al., 2007). Indeed, the transfer of limited numbers of CD4⁺ Treg cells into Treg-deficient *Foxp3^{sf}* mice is sufficient to prevent lethal inflammation in the absence of new thymic input, indicating that

mature Treg populations possess mechanisms to durably maintain their population size and function over time (Fontenot et al., 2003).

In multiple tissue types, maintenance of cellular populations is achieved by quiescent stem cells, which are capable of self-renewal while giving rise to differentiated progeny that populate the tissue and contribute to its function (Orkin and Zon, 2008). This “division of labor” between quiescent stem cells and more differentiated progeny may enable long-lived cells to protect themselves from metabolic and genomic stress associated with cellular replication and extrinsic function. Treg cells exhibit substantial heterogeneity and can be divided into resting and activated (rTreg and aTreg) cells based on the expression of T cell activation and homing molecules, including CD45RA in humans or CD62L and CD44 in mice (Benoist and Mathis, 2012; Huehn et al., 2004; Miyara et al., 2009). rTreg cells are quiescent and enriched in secondary lymphoid organs, whereas aTreg cells

¹Laboratory of Lymphocyte Signalling and Development, Babraham Institute, Cambridge, UK; ²Department of Pathology, University of Cambridge, Cambridge, UK; ³La Jolla Institute for Allergy and Immunology, La Jolla, CA; ⁴Cancer Research UK & National Institute for Health Research Experimental Cancer Sciences Unit, University of Southampton, Southampton, UK; ⁵Epigenetics DPU, Immunoinflammation Therapeutic Area Unit, GSK Medicines Research Centre, Stevenage, UK; ⁶Oregon Health and Science University School of Medicine, Portland, OR; ⁷Laboratory of Lymphocyte Differentiation, WPI Immunology Frontier Research Center, Osaka University, Osaka, Japan; ⁸Laboratory for Lymphocyte Differentiation, RIKEN Center for Integrative Medical Sciences, Yokohama, Kanagawa, Japan.

*F.M. Grant and J. Yang contributed equally to this paper; Correspondence to Jie Yang: jy437@cam.ac.uk; Rahul Roychoudhuri: rr257@cam.ac.uk.

© 2020 Grant et al. This article is distributed under the terms of an Attribution-Noncommercial-Share Alike-No Mirror Sites license for the first six months after the publication date (see <http://www.rupress.org/terms/>). After six months it is available under a Creative Commons License (Attribution-Noncommercial-Share Alike 4.0 International license, as described at <https://creativecommons.org/licenses/by-nc-sa/4.0/>).

have higher levels of suppressive function, are enriched in peripheral tissues, and are shorter lived (Cheng et al., 2012; Miyara et al., 2009). Treg cells that have recently emigrated from the thymus have an rTreg cell phenotype, suggesting that activated tTreg cells found in the periphery have arisen from resting tTreg cells (Smigiel et al., 2014), although the precise lineage relationship of the two subsets is unclear.

Signals from the TCR are now known to play a critical role in driving Treg cell heterogeneity (Li and Rudensky, 2016). Indeed, TCR signaling is required for the differentiation of rTreg cells into aTreg cells, and conditional ablation of TCR components following Treg lineage commitment results in loss of aTreg cells and an inability of the residual population of rTreg cells to limit inflammation (Levine et al., 2014; Vahl et al., 2014). The molecular mechanisms that maintain rTreg cells in their functionally quiescent state are unclear. This is a significant issue since a substantial proportion of Treg cells, including rTreg cells, have specificity for self-antigens to which they are chronically exposed in host tissues, resulting in TCR signaling that would be expected to drive aTreg differentiation. Consistent with the notion that rTreg cells frequently receive signals through the TCR is the observation that they express high levels of Nur77 ex vivo in a manner that is TCR dependent (Levine et al., 2014; Smigiel et al., 2014). The fact that rTreg cells are maintained over time and are not driven to aTreg differentiation implies that mechanisms exist to limit TCR-driven activation programs among rTreg cells.

AP-1 family TFs play a critical role in activating TCR-driven gene expression programs in lymphocytes. AP-1 TFs, including Jun, Fos, and BATF family TFs, are members of a broader basic leucine-zipper (bZip) TF family and contain bZip domains that enable them to form heterodimeric complexes at palindromic 12-O-tetradecanoylphorbol-13-acetate response elements (TREs) within genomic DNA (Glover and Harrison, 1995; Turner and Tjian, 1989). BACH2 is a transcriptional repressor of the bZip family (Igarashi et al., 2017). Through shared possession of bZip domains, BACH2 and AP-1 family members compete for binding to similar regulatory elements within genomic DNA, such that high levels of BACH2 antagonize AP-1-driven transcriptional activation by TRE (Kuwahara et al., 2016; Roychoudhuri et al., 2016a). BACH2 plays a critical role in early Treg lineage specification. Genetic ablation of BACH2 in mice results in lethal inflammation attributable to defective Treg cell development (Roychoudhuri et al., 2013). Loss of BACH2 results in a complete cell-intrinsic defect in generation of Foxp3⁺ Treg cells, as evidenced by absence of Foxp3⁺ Treg cells within the *Bach2*^{-/-} compartment of WT:*Bach2*^{-/-} mixed bone marrow (BM) chimeras. Under the inflammatory conditions present in *Bach2*^{-/-} animals, Treg cells arise, but at reduced frequencies insufficient to prevent a lethal immunoregulatory disorder (Kim et al., 2014; Roychoudhuri et al., 2013). Despite BACH2's role in early Treg lineage specification, it is unclear whether continuous BACH2 expression is required following Treg lineage commitment for maintenance of Treg lineage identity, homeostasis, or function.

In this study, we show that BACH2 is repurposed following Treg lineage commitment and restrains TCR-driven aTreg differentiation to promote the functional quiescence and long-term

maintenance of Treg cell populations. *Bach2* is highly expressed during Treg ontogeny but heterogeneously expressed among Treg cells in the periphery and down-regulated in response to inflammation. In contrast to its function before Treg lineage commitment, BACH2 is not required for maintenance of Foxp3 expression or restraint of helper cytokines within T reg cells. Rather, high levels of BACH2 expression in rTreg cells are required to restrain TCR-driven aTreg differentiation programs, maintaining their functional quiescence and promoting stable Treg population maintenance over time. Consequently, BACH2 is required under steady-state conditions to restrain excessive conventional T (Tconv) cell activation and maintain immune homeostasis. In addition, BACH2 expression within Treg cells is required to maintain the pathophysiological accumulation of Treg cells within tumors, and its conditional ablation within lineage-committed Treg cells results in induction of antitumor CD4⁺ and CD8⁺ Tconv responses and impaired tumor growth. Collectively, these findings identify BACH2 as a mechanism by which the functional quiescence of rTreg cells is maintained and for the durability of Treg cell populations during homeostasis and immunosuppression.

Results

Bach2 is heterogeneously expressed by Foxp3⁺ Treg cells in peripheral tissues and down-regulated in response to inflammation

BACH2 is required for early Treg development before Foxp3 induction, but its role following lineage commitment is unclear. We asked whether *Bach2* is expressed following Treg lineage commitment. We crossed *Foxp3*^{EGFP-DTR} animals, which express human diphtheria toxin receptor (DTR) and enhanced GFP (EGFP) under the transcriptional control of the endogenous *Foxp3* gene (Kim et al., 2007), with *Bach2*^{tdRFP} reporter animals, which express tandem RFP (tdRFP) under the transcriptional control of the endogenous *Bach2* gene (Shinnakasu et al., 2016), resulting in *Foxp3*^{EGFP-DTR} *Bach2*^{tdRFP/+} dual reporter animals. Examination of reporter expression in these animals revealed that Foxp3⁺ CD4SP cells in the thymus expressed high levels of *Bach2* (Fig. 1, A and B). However, Treg cells in peripheral tissues exhibited heterogeneous *Bach2*^{tdRFP} expression levels, with a subset of cells expressing low levels of *Bach2*^{tdRFP} (hereafter *Bach2*^{low} cells) and a subset of cells expressing high levels of *Bach2*^{tdRFP} (hereafter *Bach2*^{high} cells) when considering either total Treg cells (Fig. 1 C) or Nrp1⁺ Treg cells (Fig. 1 D), which are primarily comprised of tTreg cells under noninflammatory conditions (Yadav et al., 2012). Interestingly, the frequency of *Bach2*^{low} cells among Nrp1⁺ tTreg cells was higher than that among Nrp1⁻ pTreg cells, suggesting that tTreg cells are more susceptible to *Bach2* down-regulation than pTreg cells under steady-state conditions.

Given the heterogeneity of *Bach2* expression in the periphery, we asked whether inflammation drives down-regulation of *Bach2* expression. Limited systemic inflammation can be triggered by transient depletion of Treg cells through administration of diphtheria toxin (DTx) to *Foxp3*^{EGFP-DTR} animals, providing a well-characterized experimental system with which

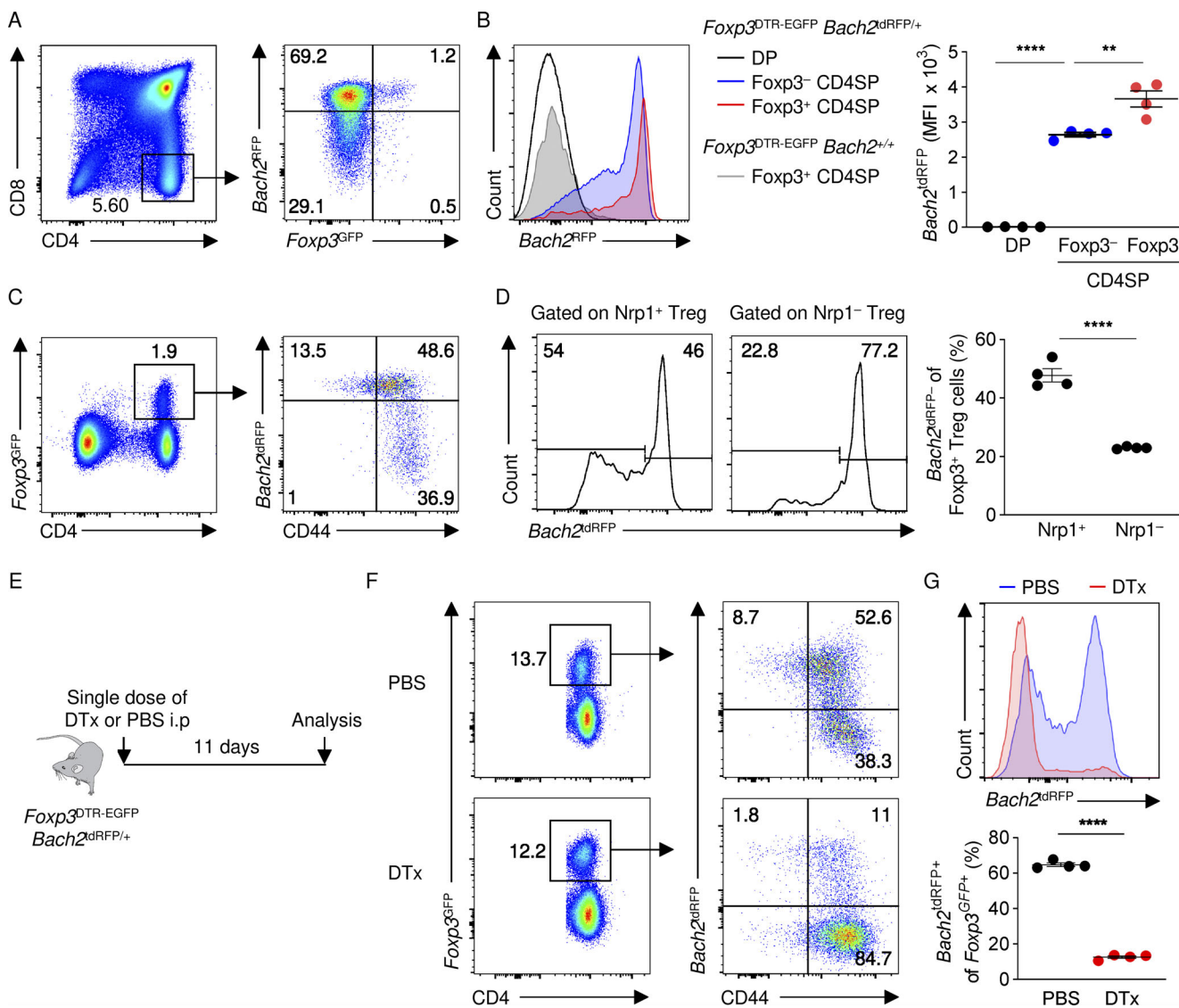


Figure 1. *Bach2* is highly expressed during Treg ontogeny but down-regulated in a subset of peripheral Treg cells in response to inflammation.

(A) Representative flow cytometry of thymocytes from *Foxp3*^{EGFP-DTR} *Bach2*^{tdRFP/+} mice, showing gating of CD4 single-positive (CD4SP) cells (left) and expression of *Bach2*^{tdRFP} and *Foxp3*^{EGFP-DTR} in these cells (right). **(B)** Histograms showing representative *Bach2*^{tdRFP} expression (left) and replicate mean fluorescence intensity measurements (right) of indicated thymocyte populations from mice of indicated genotypes. **(C)** Representative gating of splenic EGFP⁺ Treg cells isolated from *Foxp3*^{EGFP-DTR} *Bach2*^{tdRFP/+} mice (left) and expression of *Bach2*^{tdRFP} and CD44 on gated cells (right). **(D)** Representative histograms (left) and frequency of *Bach2*^{tdRFP}-low cells (right) within indicated Nrp1⁺ and Nrp1⁻ subsets of EGFP⁺ Treg cells from spleens of *Foxp3*^{EGFP-DTR} *Bach2*^{tdRFP/+} mice. **(E)** Experimental schema of the acute inflammation model in *Foxp3*^{EGFP-DTR} *Bach2*^{tdRFP/+} mice. **(F)** Representative flow cytometry of splenic EGFP⁺ Treg cells from *Foxp3*^{EGFP-DTR} *Bach2*^{tdRFP/+} mice 11 d after i.p. injection with PBS or 50 µg/kg DTx, and their expression of *Bach2*^{tdRFP} and CD44. **(G)** Representative *Bach2*^{tdRFP} expression (top) and replicate measurements (bottom) of *Bach2*^{tdRFP} expression among EGFP⁺ Treg cells after treatment. **(A–G)** Data are representative of two independently repeated experiments with four mice per group. **, P < 0.01; ****, P < 0.0001; one-way ANOVA with Tukey's adjustment for multiple testing (B) and unpaired two-tailed Student's t test (D and G). Numbers in gates show percentages. Bars and error show mean and SEM.

the response of Treg cells to systemic inflammation can be assessed (Arvey et al., 2014; Pierson et al., 2013). We administered a single dose of DTx to *Foxp3*^{EGFP-DTR/EGFP-DTR} *Bach2*^{tdRFP/+} animals and assessed expression of *Bach2*^{tdRFP} in T reg cells by flow cytometry after 11 d (Fig. 1 E). This analysis revealed a substantial reduction in the expression of *Bach2*^{tdRFP} by Treg cells after treatment of mice with DTx (Fig. 1 F and G). Taken together, we interpret these data to indicate that *Bach2* is highly expressed in Treg cells in the thymus but down-regulated in a subset of tTreg cells in peripheral tissues. Moreover, these data indicate that

Bach2 expression levels are down-regulated in response to inflammation.

High levels of *Bach2* expression mark resting Treg cells

Because BACH2 is a transcriptional repressor, we asked whether there are differences in gene expression between *Bach2*^{high} and *Bach2*^{low} Treg cells. We sorted *Foxp3*^{EGFP+} *Bach2*^{tdRFP-} and *Foxp3*^{EGFP+} *Bach2*^{tdRFP+} cells from spleens of *Foxp3*^{EGFP-DTR/EGFP-DTR} *Bach2*^{tdRFP/+} animals to high purity by FACS and subjected RNA isolated from these cells to massively parallel RNA sequencing

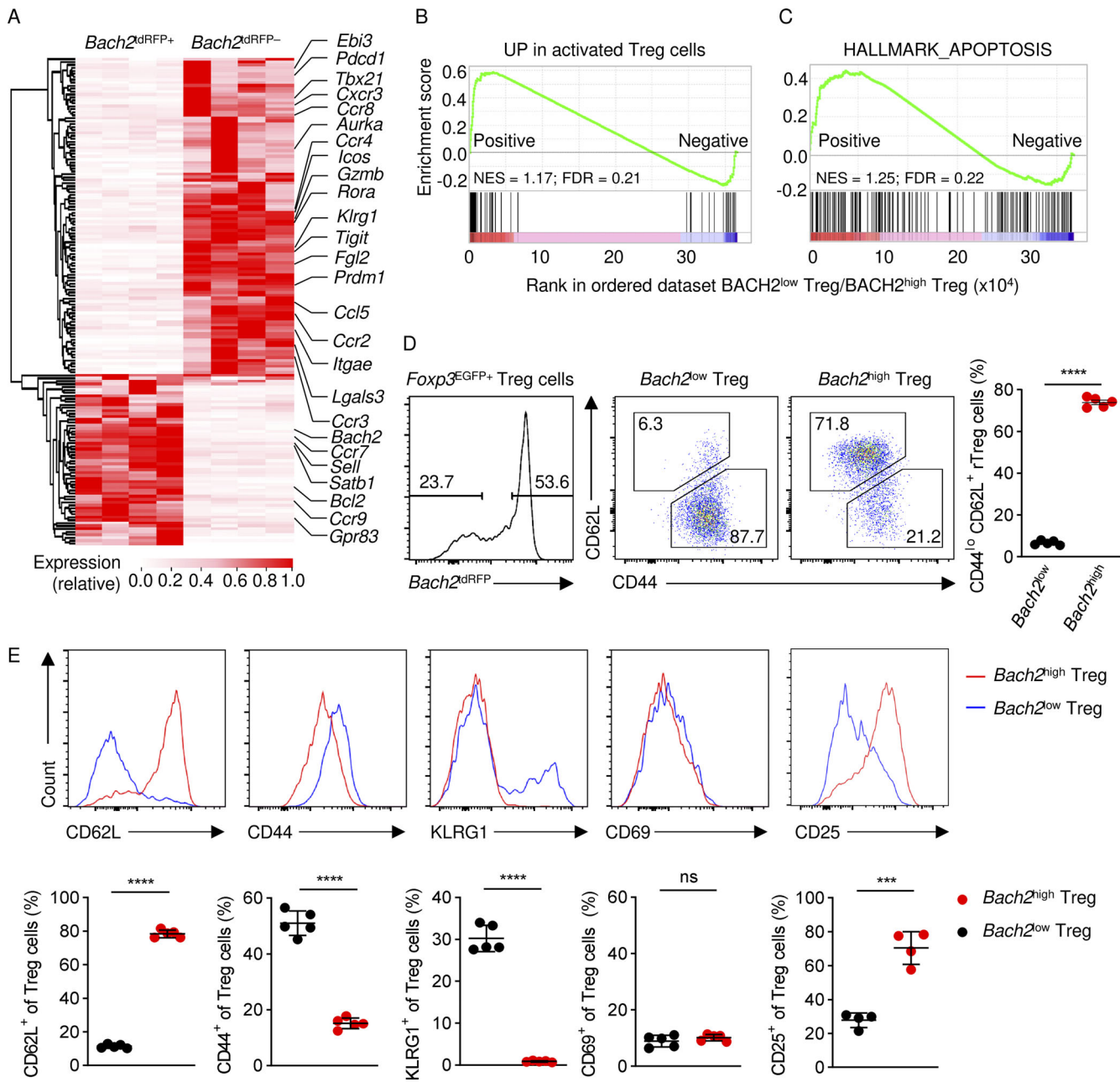


Figure 2. Heterogeneous Bach2 expression distinguishes rTreg cells and aTreg cells. **(A)** Heatmap showing differentially expressed genes between *Bach2^{high}* and *Bach2^{low}* EGFP⁺ Treg cells purified by FACS from *Foxp3^{EGFP-DTR} Bach2^{tdRFP/+}* mice (fold-change > 2, FDR < 0.05; Wald test with Benjamini-Hochberg correction). Replicates and genes are hierarchically clustered on the x and y axes, respectively. Fragments per kilobase of transcript per million mapped reads values in the heatmap are normalized to row maxima. Data are from four independent biological replicates isolated on independent days. **(B)** GSEA of known differentially up-regulated genes in aTreg cells versus rTreg cells within the global transcriptional differences between *Bach2^{low}* and *Bach2^{high}* Treg cells. **(C)** GSEA of genes involved in apoptosis within the global transcriptional differences between *Bach2^{low}* and *Bach2^{high}* Treg cells. **(D)** Representative flow cytometry (left) and replicate frequencies (right) of the expression of CD62L and CD44 on indicated Treg cell subsets from *Foxp3^{EGFP-DTR} Bach2^{tdRFP/+}* mice. **(E)** Representative histograms (top) and replicate measurements (bottom) of the expression of the indicated proteins on the surface of *Bach2^{high}* and *Bach2^{low}* Treg cells. Data are representative of two individually repeated experiments with five (D) and four to five (E) mice per group. ns, not significant; ***, P < 0.001; ****, P < 0.0001; unpaired two-tailed Student's t test (D and E). Numbers in gates show percentages. Bars and error show mean and SEM.

(RNA-Seq; Fig. 2 A and Table S1). This analysis revealed that *Bach2^{high}* cells express lower levels of genes encoding proteins involved in migration, including *Ccr4*, *Ccr2*, and *Ccl5*; costimulatory or coinhibitory signaling, including *Icos* and *Tigit*; and Treg suppressive function, including *Gzmb*, *Fgl2*, and *Prdm1*. By contrast, *Bach2^{high}* cells express higher levels of genes encoding proteins

involved in lymphoid homing, including *Sell* and *Ccr7*; a TF involved in lymphocyte quiescence, *Satb1* (Kitagawa et al., 2017); and the antiapoptotic factor *Bcl2*. Importantly, as a positive control and validation of the reporter system used, we noted higher levels of *Bach2* mRNA in *Bach2^{high}* compared with *Bach2^{low}* cells, whereas *Foxp3* mRNA was uniformly expressed.

Comparison of differences in global gene expression between *Bach2*^{high} and *Bach2*^{low} cells with known differences in gene expression between aTreg and rTreg cells using gene set enrichment analysis (GSEA; Subramanian et al., 2005) indicated that transcripts known to be up-regulated in aTreg cells compared with rTreg cells (Luo et al., 2016) were enriched among *Bach2*^{low} cells (Fig. 2 B and Table S2). Moreover, GSEA analysis indicated the up-regulation of genes associated with apoptosis among *Bach2*^{low} cells (Fig. 2 C, Table S3, and Table S4). Consistent with the above observations, we observed a higher frequency of rTreg cells among *Bach2*^{high} cells compared with *Bach2*^{low} cells (Fig. 2 D). Moreover, *Bach2*^{high} cells expressed higher levels of CD62L and CD25, lower levels of CD44 and KLRG1, and similar levels of CD69 compared with *Bach2*^{low} cells within the spleen (Fig. 2 E). Collectively, these findings indicate that heterogeneous *Bach2* expression levels discriminate Treg cells in distinct activation states, and that high levels of *Bach2* expression mark rTreg cells.

BACH2 is repurposed following Treg lineage commitment

We asked whether BACH2 exerts nonredundant functions within lineage-committed Treg cells. Because BACH2 plays a critical role in early Treg lineage commitment (Roychoudhuri et al., 2013), we wished to develop a system that would enable *Bach2* to be conditionally ablated after *Foxp3* induction. We first generated *Bach2*^{fl/fl} *Foxp3*^{YFP-Cre} animals but observed high levels of nonspecific excision of the *Bach2*^{fl} allele in non-Treg cells, consistent with previous reports of nonspecific deletion using this allele (Fig. S1 A; Andrusaité and Milling, 2020; Franckaert et al., 2015; Rubtsov et al., 2008; Wu et al., 2020). We therefore used the *Foxp3*^{EGFP-Cre-ERT2} allele, since it has been shown to drive “nonleaky” Treg-specific LoxP recombination upon administration of tamoxifen (Rubtsov et al., 2010). We confirmed the lack of nonspecific Cre activity using this allele by measuring induction of RFP fluorescence in Treg and non-Treg cells from tamoxifen-treated *Bach2*^{fl/fl} *Foxp3*^{EGFP-Cre-ERT2} *Rosa26*^{fSTOP-tdRFP} mice, in which inducible Cre activity drives deletion of a premature inactivating stop codon in the constitutively expressed RFP transgene (Luche et al., 2007; Fig. 3 A and Fig. S1 B). We also confirmed the specificity of *Foxp3*^{EGFP-Cre-ERT2} activity by measurement of the abundance of *Bach2* excision alleles in FACS-sorted non-Treg and Treg cells from *Bach2*^{fl/fl} *Foxp3*^{EGFP-Cre-ERT2} animals (Fig. 3 B). These experiments established the validity of the *Bach2*^{fl} *Foxp3*^{EGFP-Cre-ERT2} system in examining the exclusive function of BACH2 following Treg lineage specification without its nonspecific excision in other non-Treg lineages, including before Treg lineage specification.

Because BACH2 expression is required for *Foxp3* induction during Treg cell development (Kim et al., 2014; Roychoudhuri et al., 2013), we asked whether it is required for maintenance of *Foxp3* expression following Treg lineage commitment. We administered tamoxifen for 8 wk to *Bach2*^{fl/fl} *Foxp3*^{EGFP-Cre-ERT2} *Rosa26*^{fSTOP-tdRFP} animals and relevant controls, enabling indelible genetic marking of cells that had been exposed to *Foxp3*-driven Cre activity, and examined the ratio of *Foxp3*^{EGFP-} “ex-Treg” cells within the RFP⁺ CD4⁺ T cell fraction, indicating cells that had once expressed *Foxp3* but had now lost its expression

(Fig. 3 C). In both the thymus and spleen, we observed a similar ratio of *Foxp3*^{EGFP-} ex-Treg cells among the RFP⁺ fraction from *Bach2*^{fl/fl} and *Bach2*^{+/+} animals, indicating that following Treg lineage commitment, BACH2 is not required to maintain Treg lineage stability or *Foxp3* expression. Because BACH2 also restrains helper cell transcriptional programs, including helper cell cytokine production, in Tconv cells and during induced Treg (iTreg) differentiation (Roychoudhuri et al., 2013), we asked whether BACH2 restrains helper cytokine expression in lineage-committed Treg cells. We observed similar levels of IFN- γ expression by Treg cells from tamoxifen-treated *Bach2*^{+/+} *Foxp3*^{EGFP-Cre-ERT2} and *Bach2*^{fl/fl} *Foxp3*^{EGFP-Cre-ERT2} animals, indicating that BACH2 is not required for suppression of Th1 cytokine production by Treg cells (Fig. 3 D). Collectively, these results indicate that in contrast to its role before Treg lineage commitment, BACH2 is required neither to maintain *Foxp3* expression nor to restrain helper cell cytokines following Treg lineage commitment and suggest that its function is repurposed after *Foxp3* induction.

BACH2 is a global regulator of Treg population heterogeneity

To gain insight into the function of BACH2 following Treg lineage commitment, EGFP⁺ Treg cells were sorted by FACS from tamoxifen-treated *Bach2*^{+/+} *Foxp3*^{EGFP-Cre-ERT2} and *Bach2*^{fl/fl} *Foxp3*^{EGFP-Cre-ERT2} animals and subjected to single-cell RNA-Seq (scRNA-Seq) using three biological replicates per genotype. Single-cell gene expression data were clustered using Seurat and visualized in 2D space using t-distributed stochastic neighbor embedding (tSNE). This analysis revealed the presence of seven transcriptionally distinct subsets of Treg cells featuring differentially expressed genes enriched within each cluster (Fig. 4, A and B; Table S5; and Table S6). Examination of the relative frequency of WT and *Bach2*-deficient Treg cells in each cluster revealed a reduction in the frequency of *Bach2*-deficient cells in cluster 0 and cluster 1 and an increase in their ratio in cluster 4 when normalizing for the number of cells of each genotype in the analysis (Fig. 4 C). Examination of differentially expressed genes between cluster 4 and cluster 0 indicated elevated expression of genes such as *Cxcr3*, *Fgl2*, *Id2*, *Pdcld*, *Icos*, and *Casp1*, which are associated with Treg activation and were downregulated in *Bach2*^{high} versus *Bach2*^{low} cells, and decreased expression of *Sell*, *Ccr7*, and *Satb1*, which are associated with lymphoid quiescence and homing and were significantly upregulated in *Bach2*^{high} versus *Bach2*^{low} cells (Fig. 4 D and Table S7). Importantly, analysis of the effect of BACH2 on gene expression within clusters revealed only a minimal effect, with very few significantly differentially expressed genes between WT and *Bach2*-deficient cluster 0 cells (five genes at $|\log_2 \text{fold-change}| > 1$ and adjusted P [$P_{\text{adj}} < 0.05$] and between WT and *Bach2*-deficient cluster 4 cells (one gene at $|\log_2 \text{fold-change}| > 1$ and $P_{\text{adj}} < 0.05$; Table S8 and Table S9). The observation that BACH2 regulates the relative frequency of distinct clusters of cells within Treg populations while having only a minimal effect on gene expression within those clusters supports a function of BACH2 as a global regulator of the gene expression programs underlying Treg cell heterogeneity.

To assess whether BACH2 is in part responsible for the gene expression differences observed between *Bach2*^{high} and *Bach2*^{low}

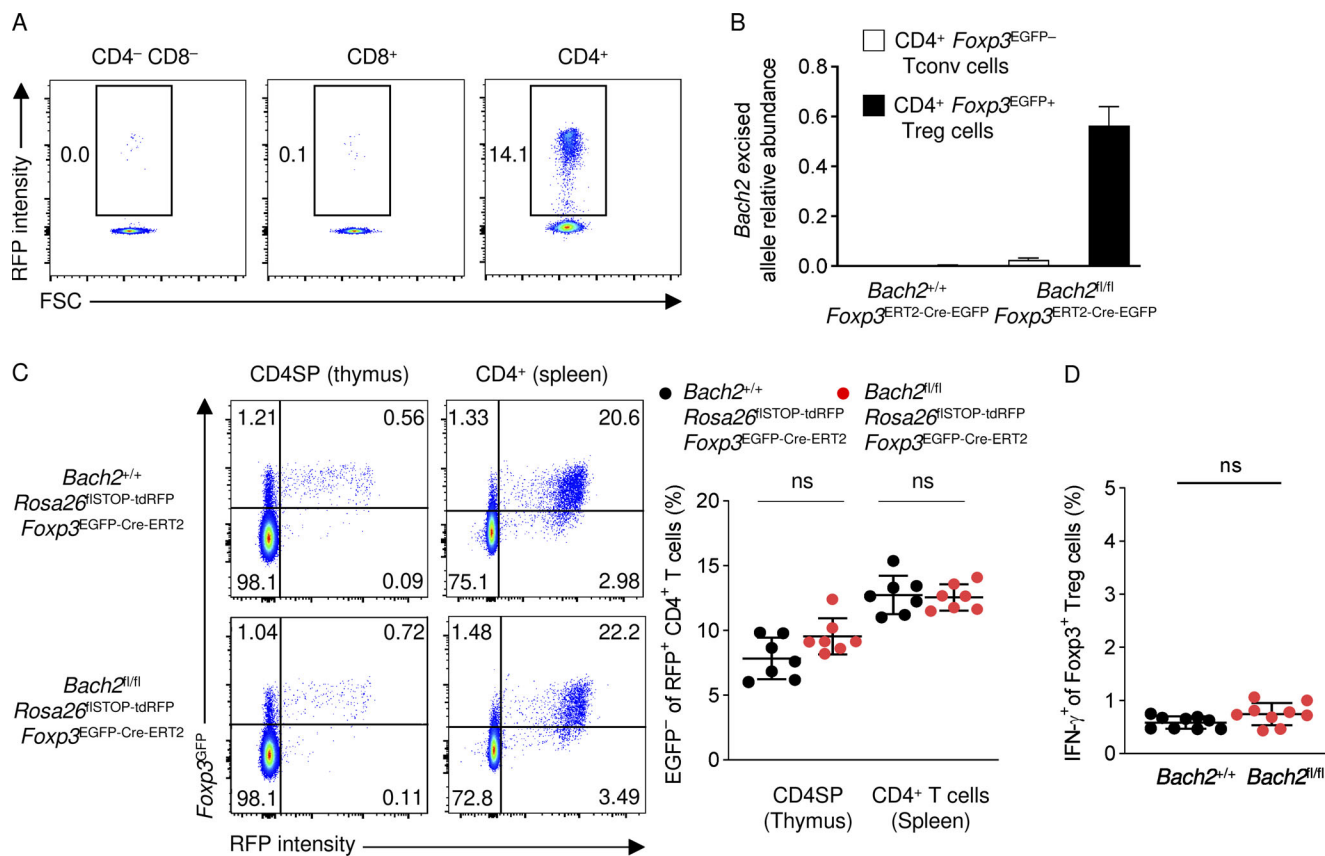


Figure 3. BACH2 is repurposed following Treg lineage commitment and is not required for maintenance of Foxp3 expression or repression of helper cytokines. (A) Representative flow cytometry plots showing *Rosa26*^{iSTOP-tdRFP} induction in CD4- CD8- lymphocytes and CD8+ or CD4+ T cells from *Bach2*^{fl/fl} *Foxp3*^{ERT2-Cre-EGFP *Rosa26*^{iSTOP-tdRFP} mice administered tamoxifen for 8 wk. (B) Quantitation of relative *Bach2* excised allele abundance in FACS-purified CD4+ *Foxp3*- Tconv and CD4+ *Foxp3*+ Treg cells isolated from the spleens of animals of indicated genotypes administered tamoxifen for 8 wk. (C) Representative flow cytometry (left) and replicate measurements (right) of the frequency of EGFP- (ex-Treg) cells within RFP+ CD4SP thymocytes or CD4+ splenocytes of mice of indicated genotypes fed tamoxifen for 8 wk. Data show seven mice per genotype. (D) Frequency of IFN- γ + Treg cells isolated from spleens of *Bach2*^{+/+} *Foxp3*^{ERT2-Cre-EGFP} mice (*Bach2*^{+/+}) and *Bach2*^{fl/fl} *Foxp3*^{ERT2-Cre-EGFP} mice (*Bach2*^{fl/fl}) given tamoxifen feed for 8 wk. Data show seven mice per genotype. (A–D) Data are representative of two independently repeated experiments. ns, not significant; unpaired two-tailed Student's t test (C and D). Numbers in gates show percentages. Bars and error show mean and SEM.}

Treg cells, we performed GSEA, which indicated that genes that were more highly expressed in *Bach2*^{low} cells than *Bach2*^{high} cells were significantly up-regulated among *Bach2*-deficient Treg cells as measured by bulk RNA-Seq analysis (Fig. 4, E and F; and Table S10). Collectively, these results indicate that BACH2 is a regulator of Treg cell heterogeneity that is required for maintenance of cells with the transcriptional properties of rTreg cells.

BACH2 represses genes associated with aTreg differentiation

To gain insight into how BACH2 functions, we examined genome-wide BACH2 binding in Treg cells. To obtain sufficient numbers of cells for this assay, we stimulated naive CD4+ T cells with plate-bound anti-CD3 and anti-CD28 antibodies in the presence of TGF- β and IL-2 for 4 d to generate iTreg cells, which were then subjected to chromatin immunoprecipitation with sequencing (ChIP-Seq). This assay revealed 9,133 BACH2 binding sites within iTreg cells, which were predominantly distributed within intronic and intergenic regions (Fig. 5 A and Table S11). Consistent with the transcriptional repressor function of BACH2, we observed a global decrease in the expression of genes

with at least one BACH2 binding site within 50 kb of their transcription start sites (TSS) in *Bach2*-proficient compared with *Bach2*-deficient cells (Fig. 5 B and Table S12). BACH2 binding sites were observed in the vicinity of a majority of genes up-regulated in Treg cells in the absence of BACH2, including *S100a11*, *Klrg1*, *Ccr4*, *Ttc39c*, *S100a4*, *Tigit*, *Fgl2*, *Ccr2*, and *Ctla2a* (Fig. 5, C and D; and Fig. S2 A). Moreover, ATAC-Seq analysis of *Bach2*-proficient and *Bach2*-deficient Treg cells revealed changes in chromatin accessibility indicative of their altered differentiation state (Fig. S2 B and Table S13). However, we did not observe an enrichment of these changes at BACH2 binding sites (Fig. S2 C). This suggests that BACH2 does not directly cause changes in the accessibility of the loci it binds, consistent with the function of a passive transcriptional repressor (Igarashi et al., 2017).

BACH2 is a steric repressor of AP-1-driven gene expression programs in Treg cells

To gain understanding of the mechanism by which BACH2 regulates gene expression within lineage-committed Treg cells,

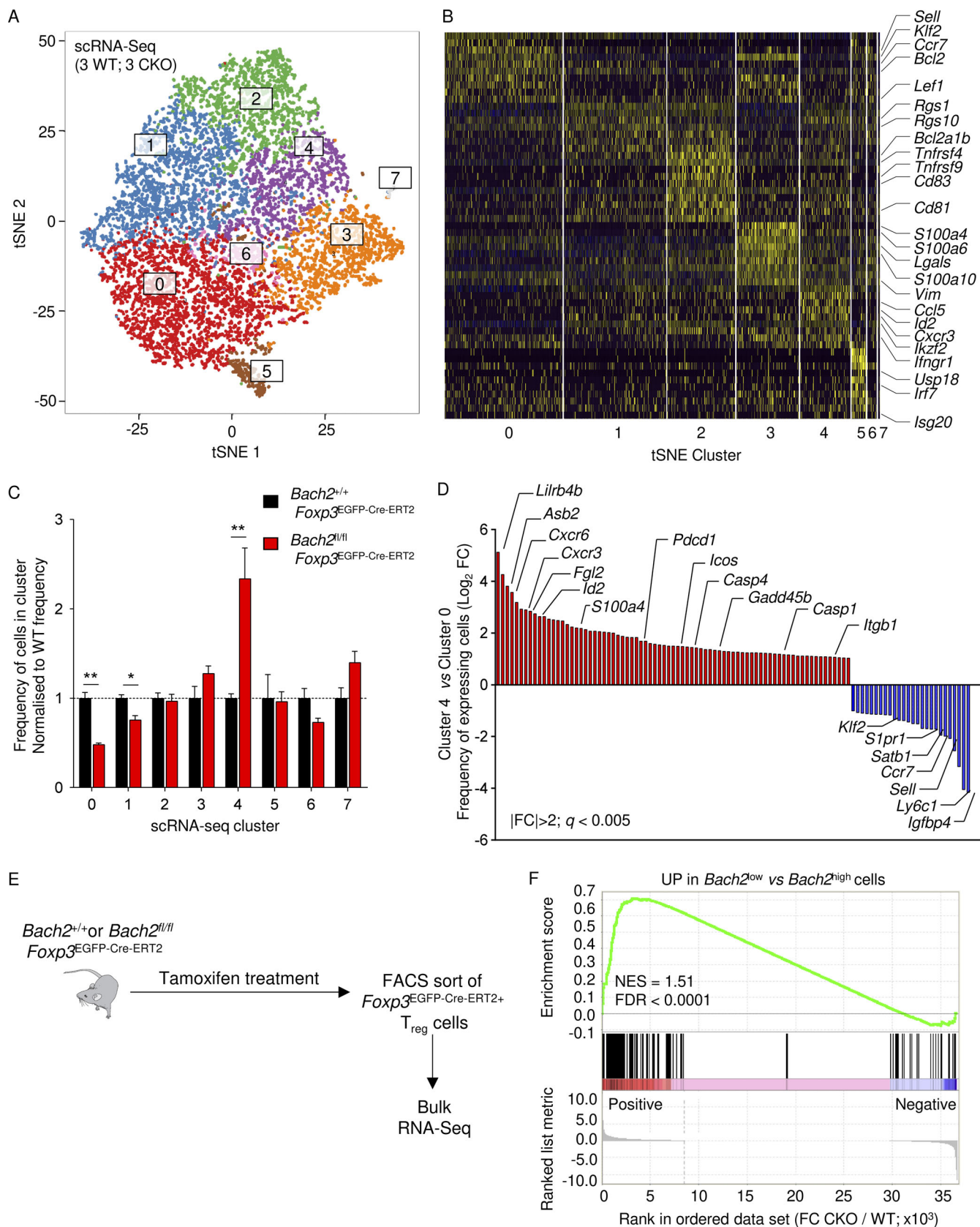


Figure 4. Single-cell and bulk RNA-Seq analysis of WT and Bach2-deficient Foxp3⁺ Treg cells. (A) tSNE representation clustered by gene expression profiles of single EGFP⁺ Treg cells isolated from the spleens of tamoxifen-treated $Bach2^{+/+}$ $Foxp3^{\text{EGFP-Cre-ERT2}}$ (WT) mice and $Bach2^{\text{fl/fl}}$ $Foxp3^{\text{EGFP-Cre-ERT2}}$ (CKO) mice. Three biological replicate cell populations per genotype were subjected to scRNA-Seq. (B) Heatmap showing the expression of the top 10 differentially

expressed genes in each cluster identified in A. (C) The relative frequency of Treg cells of indicated genotypes within each cluster normalized to their average ratio among WT replicates. (D) Graph showing the fold change in the frequency of cluster 4 versus cluster 0 cells expressing the indicated differentially expressed genes ($P_{adj} < 0.005$ and \log_2 fold-change > 1 in cluster 4 versus cluster 0). Wald test with Benjamini–Hochberg adjustment. (E and F) Experimental schema (E) and results of GSEA analysis (F) demonstrating enrichment of activated Treg cell genes in CKO versus WT cells isolated from spleens of tamoxifen-treated *Bach2^{+/+}* *Foxp3^{EGFP-Cre-ERT2}* and *Bach2^{f/f}* *Foxp3^{EGFP-Cre-ERT2}* animals. (A–F) Data from three independent biological replicates per genotype are shown. *, $P < 0.05$; **, $P < 0.01$; unpaired two-tailed Student's t test (C). Bars and error show mean and SEM.

we examined sequence motifs enriched within BACH2 binding sites. This identified a BACH2 consensus binding motif in Treg cells, which was similar to that reported for AP-1 TFs (Fig. 6 A). To test whether BACH2 competes for AP-1 sites in Treg cells, we first measured genome-wide occupancy of canonical AP-1 factor JunD in iTreg cells using ChIP-Seq (Table S14). A significant fraction of BACH2 binding sites overlapped with those of JunD (Fig. 6 B and Table S15), resulting in global colocalization of the two factors (Fig. 6 C) including at putative regulatory elements of the genes *Ctla4*, *Il10*, and *Lamc1* (Fig. 6 D). Because BACH2 has been proposed to function as a steric inhibitor of AP-1-driven gene expression in lymphocytes (Igarashi et al., 2017; Roychoudhuri et al., 2016a), we wished to examine whether AP-1 binding increases in the absence of BACH2. We isolated naive CD4⁺ T cells by FACS from *Bach2^{+/+}* *Foxp3^{EGFP-Cre-ERT2}* and *Bach2^{f/f}* *Foxp3^{EGFP-Cre-ERT2}* animals and cultured them under iTreg conditions in the presence of 4-hydroxytamoxifen. JunD binding was measured by ChIP-qPCR within these cells after brief (2 h) plate-bound anti-CD3 antibody restimulation. This analysis revealed increased binding of JunD at putative regulatory elements of *Ctla4*, *Il10*, and *Lamc1* in tamoxifen-treated *Bach2^{f/f}* *Foxp3^{EGFP-Cre-ERT2}* iTreg cells compared with *Bach2^{+/+}* *Foxp3^{EGFP-Cre-ERT2}* controls (Fig. 6 E). Consistent with increased AP-1 binding at the putative regulatory elements of these genes, we noted that their expression is increased upon stimulation of *Bach2*-deficient CD4⁺ T cells under iTreg conditions (Fig. 6 F; Sidwell et al., 2020). Taken together, the observed inhibition of JunD binding in the absence of a substantial direct effect upon chromatin accessibility supports a model in which BACH2 functions primarily as a steric repressor of AP-1-driven transcription in lymphocytes (Igarashi et al., 2017; Roychoudhuri et al., 2016a).

BACH2 restrains TCR-driven aTreg differentiation from rTreg precursors

Repression of AP-1 binding by BACH2 within Treg cells led us to ask whether BACH2 restrains the TCR-driven differentiation of rTreg cells into aTreg cells. To test this, resting CD62L⁺ EGFP⁺ Treg cells were isolated by FACS from *Bach2^{+/+}* *Foxp3^{EGFP-Cre-ERT2}* and *Bach2^{f/f}* *Foxp3^{EGFP-Cre-ERT2}* animals and cultured in the presence of IL-2, TGF-β, and 4-hydroxytamoxifen, before TCR stimulation with plate-bound anti-CD3 and anti-CD28 antibodies (Fig. 7 A). Whereas both *Bach2*-proficient and deficient rTreg cells maintained their resting phenotype in the absence of TCR signaling, we observed increased aTreg differentiation among *Bach2*-deficient cells following TCR stimulation, as indicated by increased frequencies of CD44⁺ CD62L⁻ aTreg cells, increased CD44 and CD25 expression at high levels of stimulation, and increased CTLA-4 expression at both low and high levels of

stimulation (Fig. 7, B and C). The observation that excessive aT reg differentiation caused by BACH2 deficiency requires TCR stimulation and does not occur spontaneously supports the notion that BACH2 limits TCR-driven transcriptional programs in Treg cells, a function consistent with binding of AP-1 sites in Treg cells and repression of associated genes.

BACH2 restrains aTreg differentiation in vivo and is required for long-term maintenance of Treg cell populations

In vitro analyses indicated that BACH2 restrains TCR-driven differentiation of aTreg cells from rTreg precursors. We therefore asked whether BACH2 is required for maintenance of rTreg cell quiescence in vivo. *Foxp3* is encoded on the X chromosome and is therefore subject to random X-inactivation. As a result, female mice heterozygous for *Foxp3^{EGFP-Cre-ERT2}* allele are natural chimeras containing a mixture of EGFP-Cre-ERT2-expressing and nonexpressing cells, permitting analysis of the cell-intrinsic effect of gene deletion in the presence of normally functioning Treg cells (Fig. 8 A). We therefore analyzed the phenotype of EGFP⁺ Treg cells from tamoxifen-treated naturally chimeric *Bach2^{f/f}* *Foxp3^{EGFP-Cre-ERT2/+}* animals and *Bach2^{+/+}* *Foxp3^{EGFP-Cre-ERT2/+}* controls. This analysis revealed a decrease in the proportion of CD44^{low} CD62L^{high} rTreg cells within the EGFP⁺ Treg fraction and an increase in inducible T cell costimulator (ICOS) expression after 2 wk of tamoxifen treatment. Thus, the cell-intrinsic function of BACH2 following Treg lineage specification in vivo is to restrain aTreg differentiation of rTreg precursors (Fig. 8, B and C).

Adoptive transfer experiments indicate that rTreg cells are long-lived (Cheng et al., 2012). Consistent with a role of BACH2 in rTreg homeostasis and Treg population maintenance, although there were no significant differences in the frequency of EGFP⁺ Treg cells among CD4SP thymocytes of *Bach2^{f/f}* *Foxp3^{EGFP-Cre-ERT2/+}* animals treated with tamoxifen for 8 wk, there were significantly decreased frequencies of EGFP⁺ Treg cells among CD4⁺ T cells within both the spleen and blood of these animals (Fig. S3 A). Consistently, time course measurements demonstrated a decline in the frequency of EGFP⁺ Treg cells over time following tamoxifen treatment of *Bach2^{f/f}* *Foxp3^{EGFP-Cre-ERT2/+}* animals compared with *Bach2^{+/+}* *Foxp3^{EGFP-Cre-ERT2/+}* controls (Fig. 8, D and E). This phenotype is dissimilar to the complete cell-intrinsic defect in *Foxp3⁺* Treg cell differentiation in both the thymus and periphery when BACH2 is ablated before Treg lineage specification using a previously described germline *Bach2* knockout allele (Roychoudhuri et al., 2013). To ensure that the difference between these two phenotypes resulted from differences in the timing of *Bach2* ablation relative to *Foxp3* induction rather than allele-specific differences, we

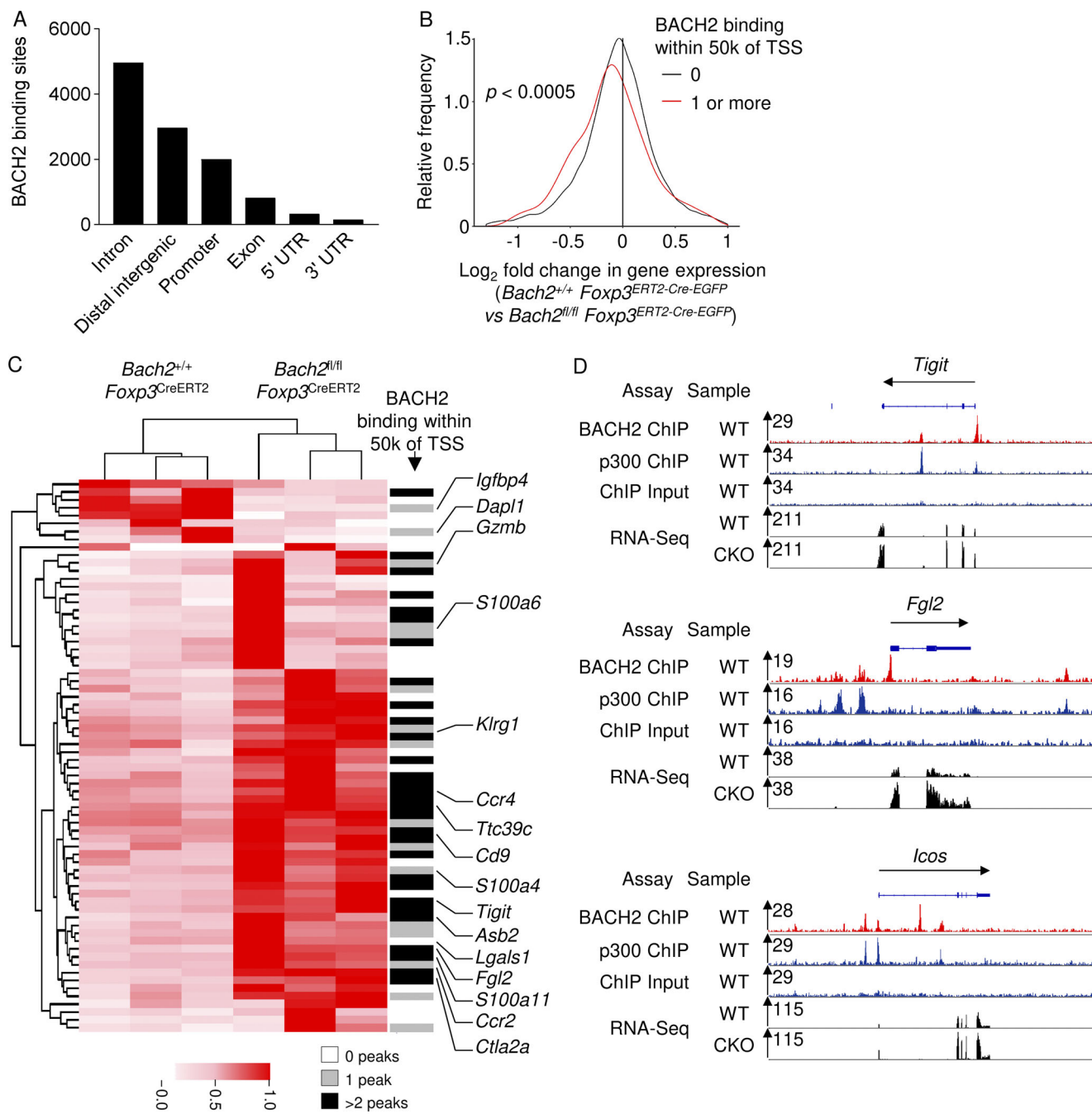


Figure 5. BACH2 represses genes associated with aTreg differentiation. **(A)** Distribution of genome-wide BACH2 binding sites identified by ChIP-Seq in iTreg cells relative to annotated features of known genes. Peaks called based on enrichment of ChIP-Seq reads over input reads (binomial distribution FDR < 5%). **(B)** Histogram showing differences in gene expression as measured by bulk RNA-Seq of all expressed transcripts within EGFP⁺ Treg cells from tamoxifen-treated animals of the indicated genotypes. Transcripts are categorized into those that do not have, or have one or more, BACH2 binding sites within 50 kb of their TSS (binomial distribution FDR < 5% and fivefold enrichment over input). Significant difference in the distribution of BACH2-bound and nonbound genes was assessed using Wilcoxon rank sum test with continuity correction. **(C)** Heatmap showing expression of differentially expressed genes in Treg cells from animals of indicated genotypes (fold-change > 1.5, FDR < 0.2; Wald test with Benjamini–Hochberg correction). Frequency of BACH2 binding sites within 50 kb of TSS of identified genes indicated to the right of the expression heatmap. Fragments per kilobase of transcript per million mapped reads normalized to row maxima. Replicates and genes are hierarchically clustered on the x and y axes, respectively. Peaks called based on enrichment over input (binomial distribution FDR < 5% and 20-fold enrichment over input). **(D)** Representative alignments of ChIP-Seq measurements showing binding of BACH2 and p300 at the indicated gene loci, and RNA-Seq measurements from EGFP⁺ Treg cells of tamoxifen-treated *Bach2*^{+/+} *Foxp3*^{ERT2-Cre-EGFP} (WT) and *Bach2*^{fl/fl} *Foxp3*^{ERT2-Cre-EGFP} (CKO) animals; RNA-Seq from three independent biological replicates per genotype are shown.

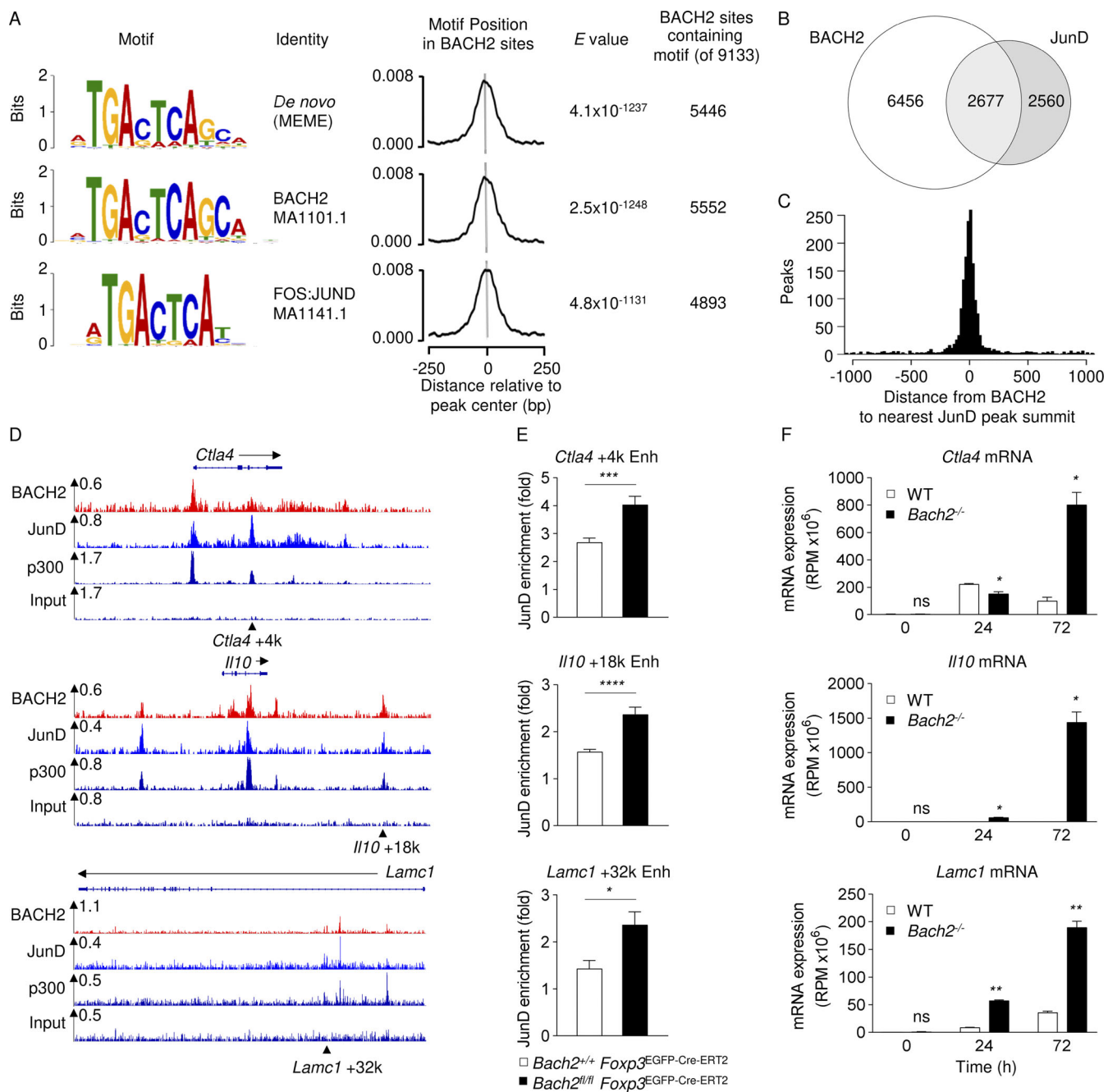


Figure 6. BACH2 restrains TCR-driven AP-1 binding in Treg cells. **(A)** De novo consensus motif (top motif) and selected known motifs from the JASPAR database (bottom motifs) enriched within BACH2 binding sites in iTreg cells (binomial distribution FDR < 5%). Average motif positions relative to BACH2 peak centers, the significance of their enrichment within BACH2 binding sites, and the number BACH2 binding sites containing the specified motifs (of 9,133 total sites) are shown. *E* values, multiple hypergeometric test using randomly shuffled input sequences. **(B)** Genome-wide colocalization analysis of BACH2 and JunD binding sites (binomial distribution FDR < 5%) in iTreg cells. The number of overlapping and nonoverlapping sites are shown by the Venn diagram. **(C)** Colocalization histogram showing the distribution of distances between BACH2 peak summits and nearest JunD peak. **(D)** Representative alignments of ChIP-Seq measurements showing binding of BACH2, JunD, and p300 at the indicated gene loci. Selected putative regulatory elements at which BACH2 and JunD bind are indicated with arrows. **(E)** Enrichment of JunD at the indicated putative regulatory elements in naive FACS-sorted CD4⁺ T cells from Bach^{+/+} Foxp3^{EGFP-Cre-ERT2} and Bach^{fl/fl} Foxp3^{EGFP-Cre-ERT2} animals cultured under iTreg conditions in the presence of 4-hydroxytamoxifen. Input-normalized JunD enrichment was assessed by ChIP-qPCR after brief (2 h) stimulation with anti-CD3 relative to negative control locus Ankrd52. Data representative of two pooled experiments with two culture replicates per genotype. **(F)** Analysis of known changes in mRNA expression following stimulation of WT or Bach2-deficient naive CD4⁺ T cells cultured under iTreg conditions and harvested at the indicated time points (Sidwell et al., 2020). ns, not significant; *P < 0.05; **P < 0.01; ***P < 0.001; ****P < 0.0001; Wilcoxon–Mann–Whitney test (E) and unpaired two-tailed Student’s *t* test (F). Numbers in gates show percentages. Bars and error show mean and SEM.

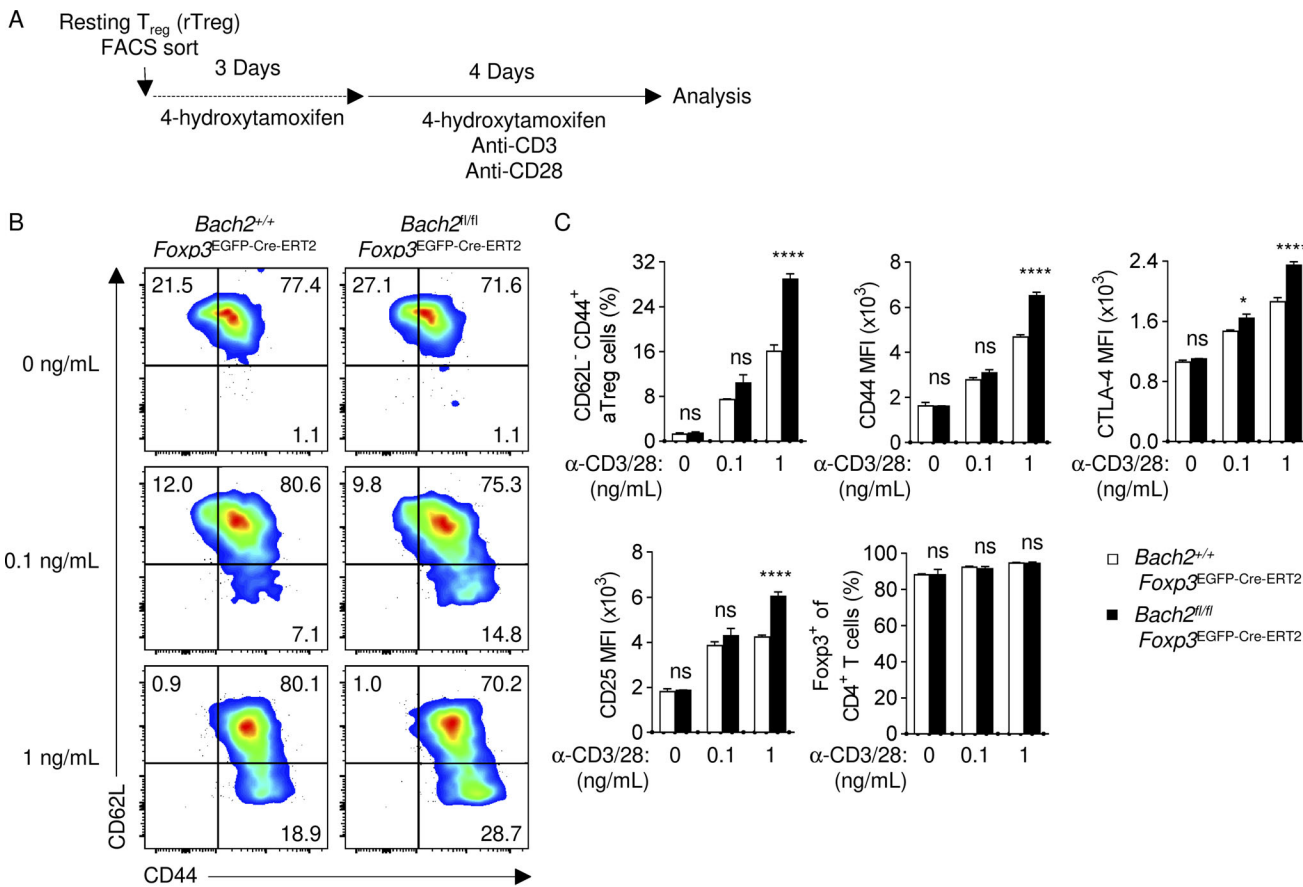


Figure 7. BACH2 restrains TCR-driven aTreg differentiation from rTreg precursors. (A) Experimental rTreg activation assay schema. Resting CD62L⁺ EGFP⁺ Treg cells were purified by FACS from spleens of animals and cultured in the presence of the indicated conditions. (B) Representative flow cytometry plots showing cell surface CD62L and CD44 expression by cells of indicated genotypes without or with stimulation with plate-bound anti-CD3 and anti-CD28 monoclonal antibodies. (C) Replicate measurements of the phenotype of Treg cells of indicated genotypes at the end of the assay. (B and C) Data are representative of two independently repeated experiments with four replicates per genotype. ns, not significant; *, P < 0.05; ***, P < 0.001; unpaired two-tailed Student's t test (C). Numbers in gates show percentages. Bars and error show mean and SEM.

confirmed that germline excision of the *Bach2*^{fl/fl} allele used in our experiments resulted in a complete cell-intrinsic defect in the generation of Treg cells in both the thymus and periphery, resembling the phenotype caused by the *Bach2* knockout allele (Fig. S3 B). Thus, BACH2 is required in a cell-intrinsic fashion for the quiescence and long-term maintenance of Treg populations *in vivo*.

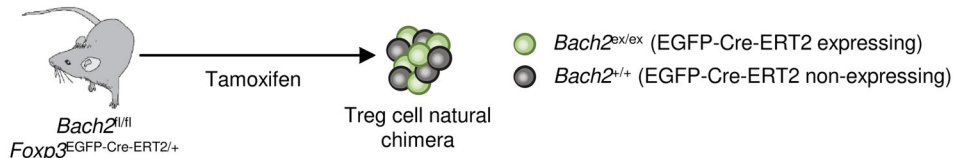
BACH2 expression in lineage-committed Treg cells is required for immune homeostasis

To test the Treg-intrinsic function of BACH2 in immune homeostasis, we examined the phenotype and function of CD4⁺ and CD8⁺ Tconv cells in *Bach2*^{fl/fl} *Foxp3*^{EGFP-Cre-ERT2} animals and *Bach2*^{+/+} *Foxp3*^{EGFP-Cre-ERT2} controls, each treated with tamoxifen. We observed increased frequencies of activated CD44⁺ CD8⁺ T cells, predominantly comprising CD44⁺ CD62L⁺ central memory cells, in the spleen and inguinal lymph nodes of *Bach2*^{fl/fl} *Foxp3*^{EGFP-Cre-ERT2} animals (Fig. 9, A and B; and Fig. S4, A and B). We also observed increased ratios of CD44⁺ CD62L⁻ effector CD8⁺ T cells in the inguinal lymph nodes of these animals (Fig. S4 B). These changes were largely restricted to the CD8⁺ T cell compartment since the frequencies of naive and

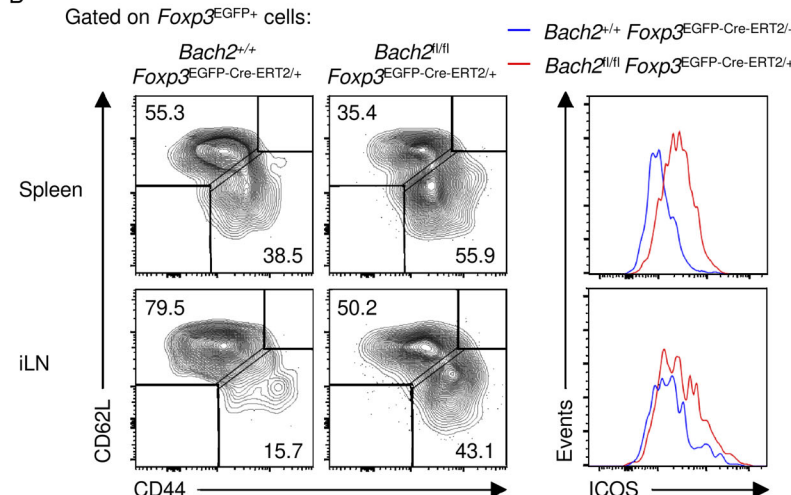
effector CD4⁺ T cells in the spleen and inguinal lymph nodes were not significantly different (Fig. S4 C). However, we did observe mildly increased ICOS expression by splenic CD4⁺ T cells (Fig. S4 D). Consistent with increased CD8⁺ T cell activation, we observed increased expression of the effector cytokine IFN-γ by CD8⁺ T cells, but not Foxp3⁻ CD4⁺ Tconv cells, from tamoxifen-treated *Bach2*^{fl/fl} *Foxp3*^{EGFP-Cre-ERT2} animals upon intracellular cytokine staining (Fig. 9 C and Fig. S4, E and F).

In the inflammatory environment of tamoxifen-treated *Bach2*^{fl/fl} *Foxp3*^{EGFP-CreERT2} animals, we observed similar frequencies of Foxp3⁺ Treg cells compared with *Bach2*^{+/+} *Foxp3*^{EGFP-CreERT2} controls (Fig. 9 D and Fig. S5 A), increased frequencies of which harbored an aTreg cell phenotype (Fig. 9 E and Fig. S5 B) and expressed high levels of ICOS (Fig. 9 F). We reasoned that the cell-extrinsic inflammatory environment present in these animals drives compensatory Treg expansion, masking the underlying cell-autonomous attrition of Treg responses that occurs in the absence of BACH2. To test this hypothesis, and to assess the background rate of Treg attrition in nonchimeric Cre-homozygous animals, we performed pulse-labeling experiments using *Bach2*^{fl/fl} *Rosa26*^{floxSTOP-tdRFP} *Foxp3*^{EGFP-CreERT2} animals

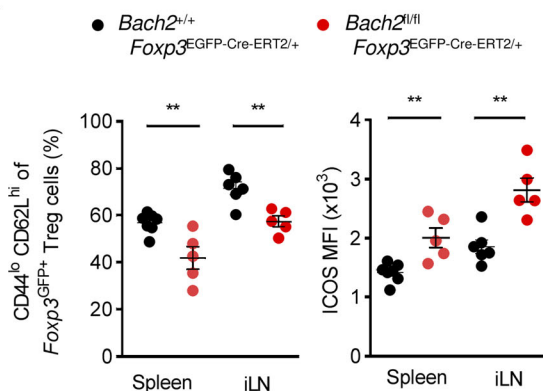
A



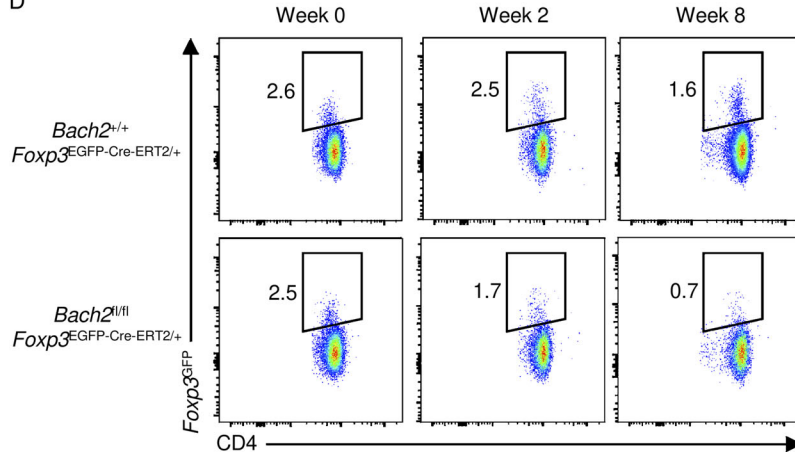
B



C



D



E

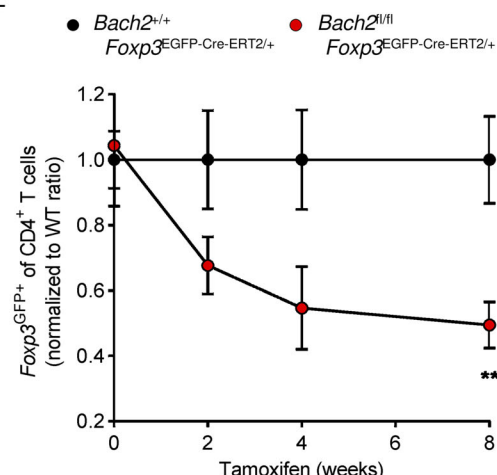


Figure 8. BACH2 restrains aTreg differentiation in a cell-intrinsic manner and is required for long-term maintenance of Treg cell populations. (A) Graphical representation of genetic heterogeneity of Treg cells from tamoxifen-treated *Foxp3^{EGFP-Cre-ERT2/+}* *Bach2^{fl/fl}* animals due to random X-inactivation. (B and C) Representative flow cytometry plots (B) and replicate measurements (C) of cell surface CD62L, CD44, and ICOS expression on EGFP⁺ Treg cells isolated from spleens and inguinal lymph nodes (iLN) of heterozygous female *Foxp3^{EGFP-Cre-ERT2/+}* *Bach2^{+/+}* or *Foxp3^{EGFP-Cre-ERT2/+}* *Bach2^{fl/fl}* mice administered tamoxifen for 2 wk. (D) Representative flow cytometry showing the frequency of EGFP⁺ Treg cells of total CD4⁺ T cells in the blood of animals at indicated time points after commencement of tamoxifen treatment. (E) Replicate measurements of EGFP⁺ Treg cells shown in D, normalized to their mean frequency in *Foxp3^{EGFP-Cre-ERT2/+}* *Bach2^{+/+}* control mice. Data are representative of two to three independently repeated experiments with five to seven (B and C) and four to five (D and E) mice per group. **, P < 0.01; unpaired two-tailed Student's t test (C and E). Numbers in gates show percentages. Bars and error show mean and SEM.

and appropriate controls (Fig. 9 G). In these animals, brief exposure to tamoxifen results in the genetic labeling of Treg cells that expressed *Foxp3* at the time of tamoxifen treatment, allowing us to label a cohort of Treg cells whose maintenance in the presence or absence of BACH2 could then be assessed in the absence of new thymic input. We observed increased attrition of *Bach2*-deficient compared with *Bach2*-proficient pulse-labeled (RFP⁺) cells as a proportion of total *Foxp3^{EGFP+}* Treg cells over time (Fig. 9 H and Fig. S5 C). These results

demonstrate that BACH2 expression within Treg cells is required for long-term maintenance of Treg populations, a function required for immune homeostasis.

BACH2 expression in lineage-committed Treg cells is required for tumor immunosuppression

T cells play a critical role in antitumor immunity, and the production of the type I cytokines IFN- γ and TNF- α is a major component of their tumoricidal function (Braumüller et al.,

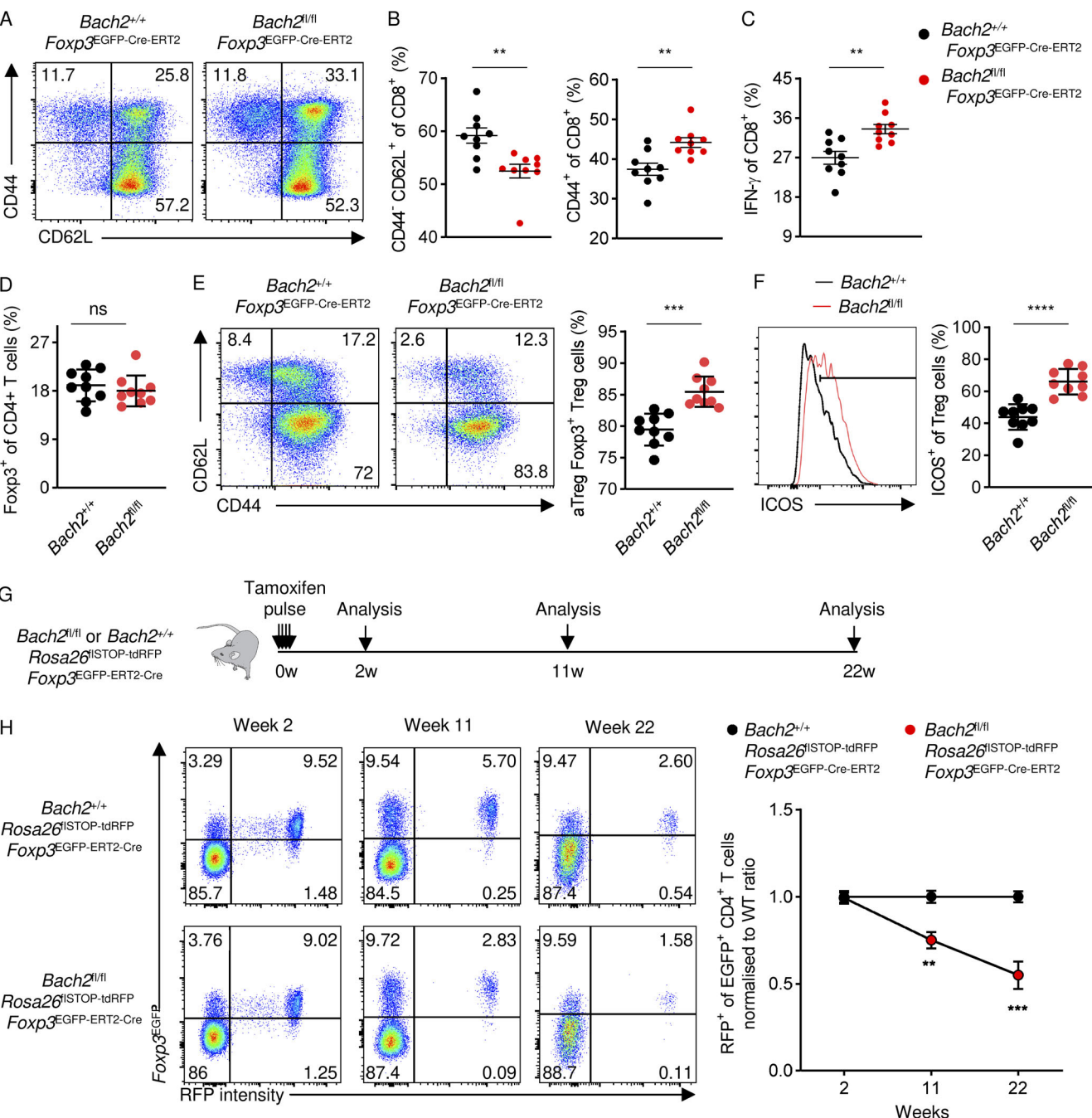


Figure 9. Treg lineage-restricted BACH2 expression is required for maintenance of immune homeostasis. **(A and B)** Representative flow cytometry showing CD44 and CD62L expression on CD8⁺ T cells (A) and frequencies of indicated CD8⁺ T cell subsets (B) within spleens of animals of the indicated genotypes treated with tamoxifen for 8 wk. **(C)** IFN- γ expression by gated CD8⁺ T cells from spleens of animals of the indicated genotypes treated with tamoxifen for 8 wk. **(D)** Foxp3 expression among CD4⁺ T cells in spleens of tamoxifen-treated nonchimeric *Foxp3^{EGFP-Cre-ERT2/EGFP-Cre-ERT2}* animals of the indicated *Bach2* genotypes. **(E)** Representative flow cytometry plots (left) and replicate measurements (right) of cell surface CD62L and CD44 expression by Treg cells isolated from the spleen of control and CKO mice given tamoxifen feed for 8 wk. **(F)** Representative expression (left) and replicate measurements (right) of ICOS on splenic Treg cells from animals of indicated genotypes treated with tamoxifen. **(G)** Experimental schema of pulse-labeling experiments using animals of the indicated genotypes *Bach2^{fl/fl}* *Rosa26^{fSTOP-tdRFP}* *Foxp3^{EGFP-Cre-ERT2}* administered tamoxifen by oral gavage over 4 d at the start of the experiments. **(H)** Flow cytometry measurements (left) and replicate measurements (right) of the frequency of RFP⁺ (pulse-labeled) cells within the bulk *Foxp3^{EGFP+}* Treg population in the blood of animals of the indicated genotypes at the indicated time points after the start of the pulse-labeling experiment in G. Frequencies shown are normalized to mean frequency of RFP⁺ cells of GFP⁺ Treg cells in *Bach2^{+/+}* *Rosa26^{fSTOP-tdRFP}* *Foxp3^{EGFP-Cre-ERT2}* animals. Unnormalized frequencies are shown in Fig. S5 C. Data are representative of two independently repeated experiments with nine (B–F) and five to seven (H) mice per group. ns, not significant; **, P < 0.01; ***, P < 0.005; ****, P < 0.001; unpaired two-tailed Student's t test (B–F and H). Numbers in gates show percentages. Bars and error show mean and SEM.

2013; Shankaran et al., 2001). Treg cells accumulate to high frequencies within tumors and suppress effective antitumor immunity (Quezada et al., 2011; Stockis et al., 2019; Tanaka and Sakaguchi, 2017). BACH2 plays a role in tumor immunosuppression through its function in Treg cell development (Roychoudhuri et al., 2016b), but whether its activity within lineage-committed Treg cells is required for tumor immunosuppression is not known. To test this, we implanted syngeneic MC38 colorectal adenocarcinoma cells subcutaneously into tamoxifen-treated *Bach2*^{fl/fl} *Foxp3*^{EGFP-Cre-ERT2} animals and assessed tumor growth at serial time points following implantation. We observed a striking reduction in the growth of tumors in *Bach2*^{fl/fl} *Foxp3*^{EGFP-Cre-ERT2} compared with control animals (Fig. 10 A) and a significant reduction in the mass of dissected tumors at day 33 after implantation (Fig. 10 B). This coincided with increased abundance of both CD8⁺ and CD4⁺ Tconv cells within the tumors of *Bach2*^{fl/fl} *Foxp3*^{EGFP-Cre-ERT2} animals (Fig. 10 C) and increased production of IFN- γ and TNF- α by these cells (Fig. 10 D). As a result, there was an elevated density of both CD8⁺ and CD4⁺ T cells expressing IFN- γ within tumors of *Bach2*^{fl/fl} *Foxp3*^{EGFP-Cre-ERT2} animals (Fig. 10 E). Despite the increased infiltration and activation of conventional T cells within tumors of *Bach2*^{fl/fl} *Foxp3*^{EGFP-Cre-ERT2} animals, the absolute density of Treg cells was only slightly higher (Fig. 10 F). This resulted in a decreased ratio of Treg cells to IFN- γ -expressing CD8⁺ T cells within tumors (Fig. 10 G). Thus, BACH2 functions within Treg cells to promote accumulation of Treg cells within tumors to sufficient pathophysiological ratios relative to activated Tconv cells to enable optimal suppression of antitumor immunity. Thus, in addition to its role in homeostasis, BACH2 functions within lineage-committed Treg cells to promote tumor immunosuppression.

Discussion

Multicellular organisms use a limited repertoire of TFs to drive the pleiotropy of cell type-specific and developmental stage-specific gene expression programs that are required for normal development and homeostasis. As a result, TFs are repurposed in different cell types or at different stages in development to drive distinct gene expression programs and cellular responses. Here, we show that the function of BACH2 is repurposed following Treg lineage commitment such that it is not required for maintenance of the Treg lineage program or for repression of helper cell identity after induction of *Foxp3*. The finding that BACH2 is no longer required for maintenance of the Treg lineage program is perhaps unsurprising, since we observed that a substantial proportion of Treg cells naturally express low levels of BACH2, and it would be undesirable for these activated and highly suppressive Treg cells to lose *Foxp3* expression and regulatory function.

BACH2 was required for the maintenance of rTreg cells and for the long-term survival of Treg cell populations in vivo. Importantly, we did not observe spontaneous aTreg differentiation of *Bach2*-deficient rTreg precursors in the absence of TCR signaling in vitro. Thus, it is likely that the function of BACH2 in vivo is to maintain the quiescence of rTreg cells in the

presence of TCR signaling. Because a majority of Treg cells bear reactivity against either self-antigens or innocuous foreign antigens to which they are chronically exposed, high levels of BACH2 expression in rTreg cells may provide a mechanism by which these cells remain functionally quiescent despite their chronic exposure to cognate antigens. It is highly likely that rTreg cells are required for maintenance of Treg populations over time, as is suggested by previous work showing that they are relatively long-lived compared with terminally differentiated aTreg cells in vivo (Cheng et al., 2012). It is important to note that a survival program, dependent on the TF Helios, also operates within effector Treg cells, which is required for immune homeostasis (Sebastian et al., 2016).

Consistent with previous reports, we noted that the frequency of *Foxp3*^{EGFP} Treg cells in *Bach2*^{+/+} *Foxp3*^{EGFP-Cre-ERT2} heterozygous animals was <50% of that in *Bach2*^{+/+} *Foxp3*^{EGFP-Cre-ERT2} homozygous animals, where 50% would be expected given random X chromosome inactivation. This has been attributed to a previously described hypomorphic effect of *Foxp3*^{Cre} alleles on Treg cells in competitive (chimeric) contexts (Franckaert et al., 2015; Rubtsov et al., 2010; Sebastian et al., 2016). This known phenomenon results in substantially <50% of the expected frequency of Treg cells expressing EGFP in *Foxp3*^{EGFP-Cre-ERT2} heterozygous animals. This hypomorphic effect of *Foxp3*^{Cre} alleles was not a confounder in our experiments since both control and experimental animals used throughout the study had the same *Foxp3*^{EGFP-Cre-ERT2} genotype between groups. These observations underscore the importance of controlling for Cre-mediated effects when choosing experimental controls.

It has recently been proposed that by preventing premature differentiation of fully suppressive effector Treg (eTreg) cells, BACH2 serves a proinflammatory function within Treg cells (Sidwell et al., 2020). Supportive of this, conditional ablation of *Bach2* in Treg cells using the *Foxp3*^{YFP-Cre} model resulted in enhanced control of dextran sodium sulfate–driven colitis in mice. We found that whereas tamoxifen-treated *Bach2*^{fl/fl} *Foxp3*^{EGFP-Cre-ERT2} animals had greater frequencies of aTreg cells, they exhibited increased steady-state CD8⁺ T cell activation and augmented antitumor immunity, a process accompanied by the attrition of pulse-labeled Treg cells over time. This is suggestive of a division of labor between rTreg cells and aTreg cells in Treg population maintenance and function, respectively. Thus, the net consequence of BACH2 function within the Treg lineage may be context-dependent: restraining short-term Treg function to sustain longer-term suppressive responses.

Whereas aTreg cells are the predominant suppressive population infiltrating tumors (Luo et al., 2016), it is reasonable to hypothesize that rTreg cells, either in tumors or in secondary lymphoid organs, form a durable source for sustained immunosuppressive Treg responses. We found that BACH2 was required for Treg cells to accumulate to normal pathophysiological ratios within tumors, as indicated by reduced frequencies of Treg cells to IFN- γ -expressing CD8⁺ Tconv cells in tumors upon Treg-specific *Bach2* ablation. In human tumors, the frequency of FOXP3⁺ cells relative to CD3⁺ or CD8⁺ Tconv cells is negatively correlated with survival in multiple cancer types, including renal cell carcinoma (Griffiths et al., 2007), non-small cell lung

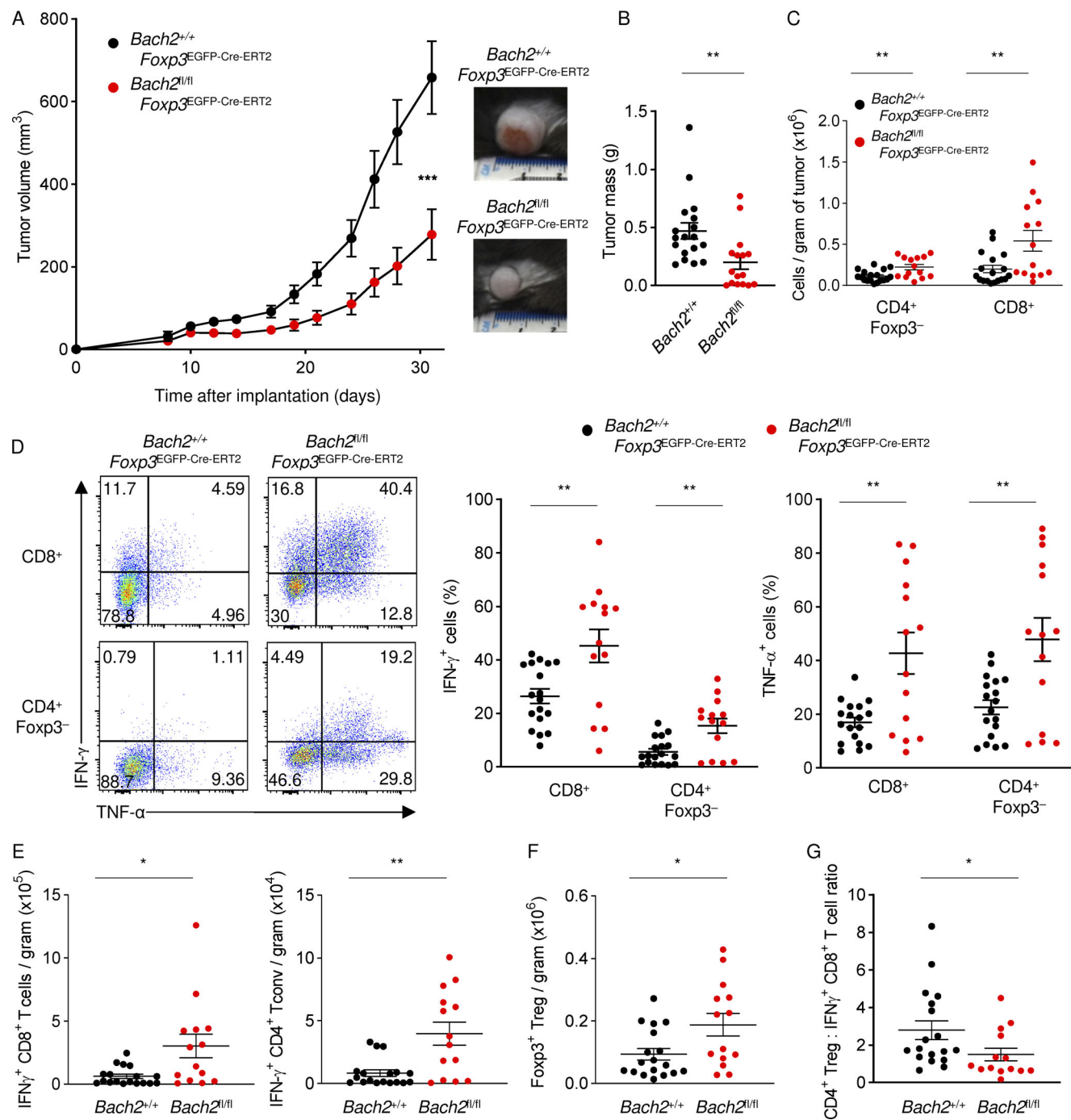


Figure 10. Treg lineage-restricted BACH2 expression is required for tumor immunosuppression. (A) Volume (left) and representative photographs (right) of tumors at the indicated time points following subcutaneous implantation of 3×10^5 MC38 colorectal adenocarcinoma cells into the flanks of tamoxifen-treated animals of the indicated genotypes. (B) Mass of tumors dissected from euthanized $Foxp3^{EGFP-Cre-ERT2}$ animals of the indicated *Bach2* genotype on day 33 after implantation. (C) CD4 $^{+}$ and CD8 $^{+}$ Tconv density within tumors on day 33 after implantation. (D) Representative flow cytometry (left) and replicate measurements (right) of the frequency of IFN- γ - and TNF- α -expressing CD8 $^{+}$ and CD4 $^{+}$ Tconv cells following brief ex vivo restimulation of tumor-infiltrating lymphocytes with PMA/ionomycin in the presence of brefeldin A. (E) Density of IFN- γ -expressing CD8 $^{+}$ and CD4 $^{+}$ Tconv cells within tumors on day 33 after implantation. (F) Density of CD4 $^{+}$ Foxp3 $^{+}$ Treg cells within tumors on day 33 after implantation. (G) Ratio of Foxp3 $^{+}$ Treg cells to IFN- γ -expressing CD8 $^{+}$ T cells within tumors on day 33 after implantation. Data are pooled from three (A) or two (B–G) independently repeated experiments with 37–40 (A) and 14–18 (B–G) mice per group. *, P < 0.05; **, P < 0.01; ***, P < 0.005; Wilcoxon–Mann–Whitney test (A, B, E, and G) and unpaired two-tailed Student's t test (C, D, and F). Numbers in gates show percentages. Bars and error show mean and SEM.

carcinoma (Petersen et al., 2006), hepatocellular carcinoma (Gao et al., 2007), pancreatic cancer (Hiraoka et al., 2006), and breast cancer (Bates et al., 2006). Thus, the pathophysiological accumulation of Treg cells is a mode of immune evasion employed by tumors. It will be important to formally test whether the accumulation of mainly aTreg cells within tumors requires a durable rTreg precursor pool. Examining the source and lineage relationship of tumor-associated rTreg and aTreg responses, and their antigen specificity, will be important in future studies and will be aided by development of tools to track tumor antigen-specific Treg responses *in vivo*.

Genetic polymorphisms in the BACH2 locus in humans are associated with susceptibility to multiple autoimmune and allergic diseases (Igarashi et al., 2017). Heterozygous non-synonymous mutations within *BACH2* are also associated with a syndrome of primary immunodeficiency and autoimmunity termed BRIDA (BACH2-related immunodeficiency and autoimmunity; Afzali et al., 2017). Although beyond the scope of this study, it will be important to assess the relative extent to which the functions of BACH2 both in early Treg lineage specification and in the maintenance of lineage-committed Treg cells results in the spectra of disease states associated with *BACH2* polymorphisms and mutations in humans. Additionally, while we observed inflammation-driven down-regulation of *Bach2* reporter expression among *Foxp3⁺* Treg cells, the precise signals mediating this effect are unclear. A number of regulatory mechanisms operate within other lymphoid lineages to regulate *Bach2* gene expression, including suppression by the AKT/mTOR pathway and activation by the tumor suppressor Menin (Ando et al., 2016; Igarashi et al., 2017; Kuwahara et al., 2014). It will be important in future studies to examine the function of these pathways in regulation of *Bach2* expression in Treg cells and thereby in controlling the threshold for rTreg-aTreg transition in the presence of TCR signaling.

Collectively, our findings provide evidence of a function of the TF BACH2, critical to early Treg lineage specification, in the quiescence and maintenance of Treg cells following lineage commitment (for a schematic model, see Fig. S5 D). Heterogeneous expression of *Bach2* among Treg cells distinguishes aTreg cells from rTreg cells and enables their response to TCR signals to be attenuated. The remarkable durability of Treg cell populations is required for lifelong maintenance of immune homeostasis, but also poses a major barrier to immune-mediated rejection of cancer. Our findings provide insights into the mechanisms that underpin the quiescence and longevity of Treg cells and may guide development of new therapies for inflammatory diseases and cancer.

Materials and methods

Mice and reagents

We have previously generated *Bach2^{tdRFP}* and *Bach2^{flx}* mice (Itoh-Nakadai et al., 2014; Kometani et al., 2013). *Rosa26^{fSTOP-tdRFP}*, *Foxp3^{EGFP-Cre-ERT2}*, *Foxp3^{DTR}* mice, and *Ptprc^a* (*CD45.1*) congenic mice and *Rag2*-deficient mice were obtained from Jackson Laboratory. C57BL/6J mice were provided by the Biological Support Unit at the Babraham Institute. Littermate controls or age- and

sex-matched animals were used in experiments as indicated. All mice were housed at the Babraham Institute Biological Support Unit. All animal experiments were conducted in accordance with UK Home Office guidelines and were approved by the Babraham Institute Animal Welfare and Ethics Review Board. Mice were genotyped by Transnetyx (Memphis, TN). For induction of Cre-ERT2-mediated recombination, mice were fed tamoxifen-containing food or corresponding control non-tamoxifen-containing food (TD130858; Envigo). All mice were given control non-tamoxifen-containing food for 2 wk before initiation of treatment to mitigate neophobic effects. For transient induction of Cre-ERT2-mediated recombination in tamoxifen pulse-labeling assays, mice were administered 8 mg tamoxifen (T5648; Sigma-Aldrich) dissolved in corn oil by oral gavage once a day for 4 d.

MC38 heterotopic tumor implantation model

MC38 colon carcinoma cells were purchased from Kerafast and passaged in DMEM (Invitrogen) supplemented with 10% FCS and antibiotics. Mice were fed tamoxifen-containing food for 2 wk before initiation of tumor implantation and kept on the same food until the study end points. 3×10^5 MC38 cells in 100 μ l PBS were injected subcutaneously into the right flanks of mice, and tumors were measured with digital calipers at serial time points after implantation.

Flow cytometry

Mouse tissues were mechanically dissociated through 40- μ m cell strainers (BD Biosciences). Red blood cells were lysed using ACK Lysing Buffer (Gibco). The samples were refiltered to generate a single-cell suspension before use in further analyses. Approximately 10^6 cells were taken from single-cell suspensions for surface and/or intracellular antibody staining. Samples requiring intracellular staining with antibodies for cytokines were first stimulated using PMA, ionomycin, and brefeldin A for 4 h in RPMI 1640 (Invitrogen, Thermo Fisher Scientific). Samples requiring viability staining were incubated alone with the dye in PBS, and then stained with cell surface antibodies (diluted 1/200) in FACS buffer. Cell surface phosphatidylserine was labeled using the eBioscience Annexin V Apoptosis Detection Set (Invitrogen, Thermo Fisher Scientific) according to the manufacturer's protocol. Cells were stained with intracellular antibodies diluted 1/200, using the eBioscience Foxp3/Transcription Factor Staining Buffer Set (Invitrogen, Thermo Fisher Scientific) according to the manufacturer's protocol. Samples were analyzed using the BD LSRIFortessa (BD Biosciences), and data were interpreted using FlowJo software. Antibodies used for flow cytometry are listed in Table S16.

FACS

Pre-enrichment of CD4⁺ T cells from single-cell suspensions was done using the MagniSort Mouse CD4 T cell Enrichment Kit (Invitrogen, Thermo Fisher Scientific) according to the manufacturer's protocol. Any markers required for cell sorting were stained using flow cytometry cell surface antibodies (detailed below), diluted 1/200, while cell suspensions were being labeled with the Enrichment Antibody Cocktail. Cells were filtered and

resuspended in RPMI 1640. Cell sorting was performed using a BD Influx (BD Biosciences). Cells were sorted into solutions of RPMI 1640 supplemented with 20% FBS (Sigma-Aldrich). After sorting, data were analyzed using FlowJo.

In vitro rTreg activation assays and iTreg differentiation

Resting Treg cells (EGFP^+ CD62L $^+$ CD4 $^+$) were purified from $\text{Foxp3}^{\text{EGFP-Cre-ERT2}}$ mice by total CD4 $^+$ T cell enrichment followed by FACS, as described above. Cells were then cultured at 20,000 cells per well in a 96-well plate in RPMI 1640 complete medium with 5 ng/ml TGF- β (R&D Systems, Bio-Techne), 5 ng/ml IL-2 (Peprotech), and 200 nM 4-hydroxytamoxifen (Sigma-Aldrich) for 3 d at 37°C, 5% CO₂. Cells were then transferred to a 96-well plate coated with anti-CD3ε and anti-CD28 antibodies (Invitrogen, Thermo Fisher Scientific), both at 1 $\mu\text{g}/\text{ml}$, overnight in PBS and cultured in fresh RPMI complete medium supplemented with TGF- β , IL-2, and 4-hydroxytamoxifen (same concentrations as before) for a further 4 d at 37°C, 5% CO₂. For in vitro differentiation of iTreg cells, naive CD44 $^-$ CD62L $^+$ CD25 $^-$ CD4 $^+$ T cells were purified by FACS from total CD4 $^+$ T cells preenriched by negative selection (eBioscience) from spleens and lymph nodes of 8–12-wk-old $\text{Bach2}^{+/+}$ $\text{Foxp3}^{\text{EGFP-Cre-ERT2}}$ and $\text{Bach2}^{\text{fl/fl}}$ $\text{Foxp3}^{\text{EGFP-Cre-ERT2}}$ animals. Naive CD4 $^+$ T cells were activated by plate-bound anti-CD3 and soluble anti-CD28 (5 $\mu\text{g}/\text{ml}$ each; eBioscience) in medium for 4 d in the presence of recombinant human (rh)IL-2 (5 ng/ml; R&D Systems) and rhTGF- β 1 (5 ng/ml; R&D Systems), and further expanded in rhIL-2 (10 ng/ml) and rhTGF- β 1 (5 ng/ml) for a further 3 d before cell harvest. Where indicated, 4-hydroxytamoxifen was added at 200 nM from day 3 of the culture.

DNA isolation and quantitative RT-PCR (qPCR) for quantification of *Bach2* excision allele frequency

DNA was isolated from FACS-sorted cell populations using the DNeasy Blood & Tissue Kit (Qiagen) according to the manufacturer's protocol. DNA and primers were prepared for qPCR using the SYBR Green Master Mix (Applied Biosystems) according to the manufacturer's protocol. All PCR reactions were run on a Bio-Rad CFX96 using the following primers: $\text{Bach2}^{\text{flox}}$, 5'-CCTTAATGGATTGGATGAGAAGCC-3' plus 5'-CTCTGTACA CAGTGGGATCCACGGG-3'; $\text{Bach2}^{\text{excised}}$, 5'-CCTTAATGGATTTCGG ATGAGAACGCC-3' plus 5'-CCCACCCCTGAAGATCTCTCGAGC-3'; TLR9, 5'-AGGAAGGTTCTGGGCTCAAT-3' plus 5'-TCTGTACCC CGTTTCTCTGC-3', confirming single template specificity using melting curve analysis and visualization of amplicon size and distribution with agarose gel electrophoresis. Relative abundance of excised allele frequency was calculated using the $\Delta\text{-CT}$ method with TLR9 signal for normalization.

RNA-Seq

Single-cell suspensions were purified by total CD4 $^+$ T cell enrichment and FACS, as described above, and stored in 40 μl RNAlater Stabilization Solution at -80°C. Samples were processed using the QIAshredder Kit (Qiagen) according to the manufacturer's protocol. RNA was extracted from samples using the RNeasy Plus Mini Kit (Qiagen) according to the manufacturer's protocol. RNA libraries were prepared using the

SmartSeq2 protocol on an automated Hamilton NGS-STAR library preparation system and sequenced using a HiSeq 2500 System (Illumina). The resulting FastQ files underwent quality control with FastQC, adaptor trimming with Cutadapt, and alignment to the NCBIM37 *Mus musculus* genome annotation with hisat2 using ClusterFlow pipelines. Differential gene expression analysis was performed using Cufflinks (Roberts et al., 2011), and differentially expressed genes were further analyzed using R. For correspondence of gene expression data with BACH2 binding spectra, the number of BACH2 binding sites (false discovery rate [FDR] < 0.05; 5- or 20-fold enrichment over input) within a window of 50 kb of the TSS of annotated RefSeq genes was calculated using bedtools window v2.27 and used to classify genes for differential gene expression analysis binned into subsets based on the number of BACH2 binding sites within a 50-kb interval.

scRNA-Seq and analysis

Single-cell suspensions of Treg cells were purified by total CD4 $^+$ T cell enrichment and FACS, as described above. RNA libraries were prepared for single-cell RNA sequencing (scRNA-Seq) using the Chromium Single Cell 3' Library & Gel Bead Kit v2 (10x Genomics), processed with Chromium (10x Genomics), and sequenced using the HiSeq 4000 System (Illumina). Raw 10 \times sequencing data were processed as previously described, except the data were mapped to mm10. We confirmed that cells were sequenced to saturation. Each library was down-sampled to equivalent sequencing depth and were merged with cell ranger aggr (v2.0.2). Merged data were transferred to the R statistical environment for analysis using the package Seurat (v2.3.4) in R v3.5.0. The analysis included only cells expressing between 200 and 2,500 genes, <5% mitochondrial-associated transcripts, and genes expressed in at least three cells. The data were then log-normalized and scaled per cell, and variable genes were detected using the Findvariablegenes function in Seurat, as per default settings. The transcriptomic data from each cell were then further normalized by the number of genes quantified, unique molecular identifiers detected, and mitochondrial genes to account for technical variation. Principal component analysis was run on the variable genes, and the first five principal components (PCs) were selected for further analyses, based on the standard deviation of the PCs, as determined by an "elbow plot" in Seurat. Cells were clustered using the FindClusters function in Seurat with default settings, resolution = 0.6, and five PCs. Upon initial analysis, it was identified that the majority of variance was reflective of minor B cell and myeloid contamination. These two clusters were removed (SubsetData function), the most variable genes were recalculated, the data were rescaled, and the number of PCs for further analysis were recalculated, as above. The filtered dataset was reclustered using the Findclusters function, using the first seven PCs, resolution 0.6 (default). tSNE was calculated using default perplexity and seven PCs (RunTSNE function). For broadly defining the transcriptional features of each cluster, the FindAllMarkers function (only.pos = FALSE, min.pct = 0.0, thresh.use = 0) was used, and the associated heatmap was generated using the DoHeatmap function using up to the top 10 transcripts identified per cluster as

defined by FindAllMarkers. Differential expression between cluster 4 and cluster 0 was determined using MAST v1.8.0 ($q < 0.05$, min.pct = 0, rest as per default). Further visualizations of exported normalized data were generated using Seurat and custom R scripts. Downsampling was achieved using the SubsetData function in Seurat to maintain equivalent numbers of cells between KO and WT mice libraries (5,046 cells).

ChIP-Seq

1.5×10^7 to 2×10^7 cells were chemically cross-linked and sonicated on a Branson 450-D sonicator to generate fragmented genomic DNA. ChIP was performed using the following antibodies: anti-BACH2 (N-2; Tohoku University), anti-JunD (sc-74; Santa Cruz), and anti-p300 (sc-584; Santa Cruz) and subjected to either qPCR or sequencing. For qPCR, the following primers were used: Il10_enh_Fw, 5'-TTCCCTCTTGGTCCTCC-3'; Il10_enh_Rv, 5'-ACTCCATGCCTCCTGAACTC-3'; Ctla4_enh_Fw, 5'-AAGAACACGCTAGAACCCA-3'; Ctla4_enh_Rv, 5'-CCAAAA CAGCTGCTCCATGT-3'; Lamc1_enh_Fw, 5'-GACCCCTTCTCC GTGATTGA-3'; Lamc1_enh_Rv, 5'-CACCTTATACCTTGCACC ACAG-3'; Ankrd52_Fw, 5'-ATTAACACTTGGGCCCTTGG-3'; and Ankrd52_Rv, 5'-GGACCGGGTCTGCCTATATC-3' and measured using the SYBR Green Master Mix kit (Applied Biosystems) according to the manufacturer's instructions. The fold-enrichment of input-normalized ChIP signals over negative control Ankrd52 locus was calculated using the $\Delta\Delta CT$ method. For sequencing of immunoprecipitated DNA, DNA fragments were blunt-end ligated to Illumina adaptors, amplified, and sequenced using the HiSeq 2000 platform (Illumina). Sequenced reads of 50–125 bp were obtained using the Illumina pipeline. The sequenced reads were aligned to the mouse genome (NCBIM37/mm9) with Bowtie 0.12.9; only uniquely mapped reads were retained. The output of Bowtie was converted to bam files, which represented the genomic coordinates of each read. The ChIP-Seq signal in non-overlapping 10-bp windows was calculated by merging read density mapped to either DNA strand shifted downstream by half the estimated fragment length. Genomic graphs were generated and viewed using the Integrative Genomics Viewer (Broad Institute).

Analysis of genome-wide chromatin accessibility using ATAC-Seq

Genome-wide measurement of chromatin accessibility was performed from biological replicates using ATAC-Seq of FACS-sorted CD4⁺ Foxp3^{EGFP}⁺ Treg cells isolated ex vivo as previously described (Buenrostro et al., 2013). ATAC-Seq reads were trimmed using Trim Galore (v0.4.4) using default parameters to remove standard Illumina adapter sequences. Reads were mapped to the mouse NCBIM37 genome assembly using Bowtie2 v2.3.2 with default parameters. TDF files for analysis in the Integrative Genomics Viewer genome browser were generated using Samtools v1.9 and Igvtools v2.3.26, and differential accessibility of called peaks (MACS) was assessed using Diffbind. Histograms of chromatin accessibility were generated by counting reads into binned windows (20 bp/bin) relative to peak summits. Normalized read densities were plotted centered around peak summits.

Peak calling, motif discovery, and genome-wide distribution analysis

We used MACS 2 to call binding sites (peaks) relative to input control libraries with an FDR threshold of 0.05 and indicated fold enrichment over ChIP input. For motif discovery, the DNA sequences of called peaks were analyzed using MEME to identify the BACH2 consensus binding motif in Treg cells. The discovered motifs were compared with the JASPAR motif database to evaluate motif similarities. The relationship of identified binding sites to 5' untranslated region (UTR), 3' UTR, introns, exons, and intergenic regions were defined according to the RefSeq database using the R package ChIPseeker 1.18. The distance between the summits of BACH2 and JunD peaks was calculated using bedtools closest 2.25 and plotted as histograms using ggplot2.

Statistical testing

The Shapiro-Wilk test was used to test for normality of underlying sample distributions. Data were analyzed using unpaired two-tailed Student's *t* tests where stated and when underlying normality of the sample distribution was confirmed. In cases where the underlying sample distribution was nonnormal, or where Student's *t* tests were not appropriate, Wilcoxon-Mann-Whitney or other nonparametric tests were performed as stated. No blinding was necessary since objective quantitative assays, such as flow cytometry, were used. Experimental sample sizes were chosen using power calculations, using preliminary experiments, or were based on previous experience of variability in similar experiments. Samples that had undergone technical failure during processing were excluded from analyses.

Data availability

Data are publicly available under NCBI GEO accession no. GSE128176.

Online supplemental material

Fig. S1 shows assessment of nonspecific Cre activity in *Bach2*^{fl/fl} *Foxp3*^{YFP-Cre} mice. Fig. S2 shows genome-wide analysis of chromatin accessibility in WT and *Bach2*-deficient Treg cells. Fig. S3 shows the phenotype of Foxp3⁺ Treg cells in *Bach2*^{fl/fl} *Foxp3*^{EGFP-Cre-ERT2/+} mice. Fig. S4 shows the phenotype of CD4⁺ and CD8⁺ Tconv cells in *Bach2*^{fl/fl} *Foxp3*^{EGFP-Cre-ERT2} mice. Fig. S5 shows that BACH2 after Treg lineage-specification is required for long-term maintenance of Treg populations. Table S1 shows genes up-regulated in *Bach2*^{tdRFP}-low versus *Bach2*^{tdRFP}-high Treg cells. Table S2 shows GSEA of global gene expression changes between *Foxp3*^{GFP}-positive *Bach2*^{tdRFP}-low Treg cells and *Foxp3*^{GFP}-positive *Bach2*^{tdRFP}-high Treg cells. Table S3 shows most significantly enriched hallmark gene sets in *Foxp3*^{GFP}-positive *Bach2*^{tdRFP}-low Treg cells versus *Foxp3*^{GFP}-positive *Bach2*^{tdRFP}-high Treg cells. Table S4 shows GSEA of the HALLMARK_APOPTOSIS geneset within global gene expression differences between *Bach2*^{tdRFP}-low and *Bach2*^{tdRFP}-high Treg cells. Table S5 shows scRNA-Seq frequency (percentage positive) of single cells expressing within each cluster. Table S6 shows scRNA-Seq genes exhibiting significant differential enrichment between clusters. Table S7 shows genes up-regulated in cluster 0 versus cluster 4 from tSNE analysis of

single *Foxp3*^{EGFP}-positive Treg cells. Table S8 shows differentially expressed genes between WT and *Bach2*-deficient cluster 0 Treg cells. Table S9 shows differentially expressed genes between WT and *Bach2*-deficient cluster 4 Treg cells. Table S10 shows GSEA of genes significantly up-regulated in *Bach2*^{tdRFP}-low versus *Bach2*^{tdRFP}-high Treg cells. Table S11 shows genomic locations of significantly enriched BACH2 binding sites identified by ChIP-Seq within iTreg cells. Table S12 shows gene expression in *Foxp3*^{EGFP}-positive Treg cells from *Bach2*^{+/+} *Foxp3*^{EGFP-Cre-ERT2} (WT) and *Bach2*^{fl/fl} *Foxp3*^{EGFP-Cre-ERT2} (CKO) animals treated with tamoxifen. Table S13 shows genome-wide analysis of differentially accessible chromatin in WT and CKO animals treated with tamoxifen. Table S14 shows genomic locations of significantly enriched JunD binding sites identified by ChIP-Seq within iTreg cells. Table S15 shows colocalized genomic binding sites between BACH2 and JunD within in vitro-generated iTreg cells. Table S16 lists flow cytometry antibodies.

Acknowledgments

This paper is dedicated to the memory of our wonderful friend and colleague, Professor Michael Wakelam, who recently passed away.

We thank members of the Babraham Institute Biological Services Facility including Carly Noble, Ian Horseman, Laura and Marc Wiltshire, Michael Penn, Sarah Fletcher, Nicola Evans-Bailey, Heather Large, Michael Regan, and Urszula Karpinska for technical support with animal experiments. We thank Kristina Tabbada of the Sequencing Facility for assistance with library preparation and sequencing; members of the Flow Cytometry facility, including Rachael Walker, Attila Bebes, Rebecca Roberts, and Arthur Davis, for their assistance with cell sorting and analysis; Simon Andrews of the Bioinformatics Group for guidance with data analysis; and P. Coupland and K. Kania at the Cancer Research UK Cambridge Institute for assistance with scRNA-Seq analysis. We thank Martin Turner, Michelle Linterman, Adrian Liston, Ine Vanderleyden, and Geoff Butcher from the Babraham Institute for generous sharing of reagents, support, and discussion. We apologize to any authors whose work could not be cited due to space constraints.

The research was supported by Wellcome Trust-Royal Society Fellowship 105663/Z/14/Z (R. Roychoudhuri); Biotechnology and Biological Sciences Research Council grants BB/N007794/1, BBS/E/B/000C0427, and BBS/E/B/000C0428; Cancer Research UK grant C52623/A22597; and Medical Research Council grant MR/S024468/1.

Author contributions: F.M. Grant, J. Yang, and R. Roychoudhuri wrote the manuscript and designed experiments. F.M. Grant, J. Yang, R. Nasrallah, R. Roychoudhuri, T. Todorov, C.J. Imianowski, S.K. Whiteside, I. Patrascan, P. Vardaka, P. Kuo, and N. Zandhuis performed experiments. F.M. Grant, F. Sadiyah, and J. Clarke analyzed bioinformatic data. T. Kurosaki and K. Kometani provided mouse reagents and associated protocols. D. Tough, R. Eil, and K. Okkenhaug edited the manuscript, provided protocols and support, and advised on methodology. R. Roychoudhuri supervised the work.

Disclosures: The authors declare no competing interests exist.

References

- Afzali, B., J. Grönholm, J. Vandrovčová, C. O'Brien, H.W. Sun, I. Vanderleyden, F.P. Davis, A. Khoder, Y. Zhang, A.N. Hegazy, et al. 2017. BACH2 immunodeficiency illustrates an association between super-enhancers and haploinsufficiency. *Nat. Immunol.* 18:813–823. <https://doi.org/10.1038/ni.3753>
- Ando, R., H. Shima, T. Tamahara, Y. Sato, M. Watanabe-Matsui, H. Kato, N. Sax, H. Motohashi, K. Taguchi, M. Yamamoto, et al. 2016. The Transcription Factor Bach2 Is Phosphorylated at Multiple Sites in Murine B Cells but a Single Site Prevents Its Nuclear Localization. *J. Biol. Chem.* 291:1826–1840. <https://doi.org/10.1074/jbc.M115.661702>
- Andrusaité, A., and S. Milling. 2020. Should we be more cre-tical? A cautionary tale of recombination. *Immunology*. 159:131–132. <https://doi.org/10.1111/imm.13170>
- Arvey, A., J. van der Veeken, R.M. Samstein, Y. Feng, J.A. Stamatoyannopoulos, and A.Y. Rudensky. 2014. Inflammation-induced repression of chromatin bound by the transcription factor Foxp3 in regulatory T cells. *Nat. Immunol.* 15:580–587. <https://doi.org/10.1038/ni.2868>
- Bates, G.J., S.B. Fox, C. Han, R.D. Leek, J.F. Garcia, A.L. Harris, and A.H. Banham. 2006. Quantification of regulatory T cells enables the identification of high-risk breast cancer patients and those at risk of late relapse. *J. Clin. Oncol.* 24:5373–5380. <https://doi.org/10.1200/JCO.2006.05.9584>
- Benoist, C., and D. Mathis. 2012. Treg cells, life history, and diversity. *Cold Spring Harb. Perspect. Biol.* 4: a007021. <https://doi.org/10.1101/cshperspect.a007021>
- Braumüller, H., T. Wieder, E. Brenner, S. Aßmann, M. Hahn, M. Alkhaled, K. Schilbach, F. Essmann, M. Kneilling, C. Griessinger, et al. 2013. T-helper-1-cell cytokines drive cancer into senescence. *Nature*. 494: 361–365. <https://doi.org/10.1038/nature11824>
- Buenrostro, J.D., P.G. Giresi, L.C. Zaba, H.Y. Chang, and W.J. Greenleaf. 2013. Transposition of native chromatin for fast and sensitive epigenomic profiling of open chromatin, DNA-binding proteins and nucleosome position. *Nat. Methods*. 10:1213–1218. <https://doi.org/10.1038/nmeth.2688>
- Cheng, G., X. Yuan, M.S. Tsai, E.R. Podack, A. Yu, and T.R. Malek. 2012. IL-2 receptor signaling is essential for the development of Klrg1⁺ terminally differentiated T regulatory cells. *J. Immunol.* 189:1780–1791. <https://doi.org/10.4049/jimmunol.1103768>
- Fontenot, J.D., M.A. Gavin, and A.Y. Rudensky. 2003. Foxp3 programs the development and function of CD4+CD25+ regulatory T cells. *Nat. Immunol.* 4:330–336. <https://doi.org/10.1038/ni904>
- Franckaert, D., J. Dooley, E. Roos, S. Floess, J. Huehn, H. Luche, H.J. Fehling, A. Liston, M.A. Linterman, and S.M. Schlenner. 2015. Promiscuous Foxp3^{cre} activity reveals a differential requirement for CD28 in Foxp3⁺ and Foxp3⁻ T cells. *Immunol. Cell Biol.* 93:417–423. <https://doi.org/10.1038/icb.2014.108>
- Gao, Q., S.J. Qiu, J. Fan, J. Zhou, X.Y. Wang, Y.S. Xiao, Y. Xu, Y.W. Li, and Z.Y. Tang. 2007. Intratumoral balance of regulatory and cytotoxic T cells is associated with prognosis of hepatocellular carcinoma after resection. *J. Clin. Oncol.* 25:2586–2593. <https://doi.org/10.1200/JCO.2006.09.4565>
- Glover, J.N., and S.C. Harrison. 1995. Crystal structure of the heterodimeric bZIP transcription factor c-Fos-c-Jun bound to DNA. *Nature*. 373: 257–261. <https://doi.org/10.1038/373257a0>
- Griffiths, R.W., E. Elkord, D.E. Gilham, V. Ramani, N. Clarke, P.L. Stern, and R.E. Hawkins. 2007. Frequency of regulatory T cells in renal cell carcinoma patients and investigation of correlation with survival. *Cancer Immunol. Immunother.* 56:1743–1753. <https://doi.org/10.1007/s00262-007-0318-z>
- Hiraoka, N., K. Onozato, T. Kosuge, and S. Hirohashi. 2006. Prevalence of FOXP3⁺ regulatory T cells increases during the progression of pancreatic ductal adenocarcinoma and its premalignant lesions. *Clin. Cancer Res.* 12:5423–5434. <https://doi.org/10.1158/1078-0432.CCR-06-0369>
- Huehn, J., K. Siegmund, J.C. Lehmann, C. Siewert, U. Haubold, M. Feuerer, G.F. Debes, J. Lauber, O. Frey, G.K. Przybylski, et al. 2004. Developmental stage, phenotype, and migration distinguish naive- and effector/memory-like CD4⁺ regulatory T cells. *J. Exp. Med.* 199:303–313. <https://doi.org/10.1084/jem.20031562>

- Igarashi, K., T. Kurosaki, and R. Roychoudhuri. 2017. BACH transcription factors in innate and adaptive immunity. *Nat. Rev. Immunol.* 17:437–450. <https://doi.org/10.1038/nri.2017.26>
- Itoh-Nakadai, A., R. Hikota, A. Muto, K. Kometani, M. Watanabe-Matsui, Y. Sato, M. Kobayashi, A. Nakamura, Y. Miura, Y. Yano, et al. 2014. The transcription repressors Bach2 and Bach1 promote B cell development by repressing the myeloid program. *Nat. Immunol.* 15:1171–1180. <https://doi.org/10.1038/ni.3024>
- Josefowicz, S.Z., L.F. Lu, and A.Y. Rudensky. 2012a. Regulatory T cells: mechanisms of differentiation and function. *Annu. Rev. Immunol.* 30: 531–564. <https://doi.org/10.1146/annurev.immunol.25.022106.141623>
- Josefowicz, S.Z., R.E. Nied, H.Y. Kim, P. Treuting, T. Chinen, Y. Zheng, D.T. Umetsu, and A.Y. Rudensky. 2012b. Extrathymically generated regulatory T cells control mucosal TH2 inflammation. *Nature*. 482:395–399. <https://doi.org/10.1038/nature10772>
- Kim, E.H., D.J. Gasper, S.H. Lee, E.H. Plisch, J. Svaren, and M. Suresh. 2014. Bach2 regulates homeostasis of Foxp3+ regulatory T cells and protects against fatal lung disease in mice. *J. Immunol.* 192:985–995. <https://doi.org/10.4049/jimmunol.1302378>
- Kim, J.M., J.P. Rasmussen, and A.Y. Rudensky. 2007. Regulatory T cells prevent catastrophic autoimmunity throughout the lifespan of mice. *Nat. Immunol.* 8:191–197. <https://doi.org/10.1038/ni1428>
- Kitagawa, Y., N. Ohkura, Y. Kidani, A. Vandenberg, K. Hirota, R. Kawakami, K. Yasuda, D. Motooka, S. Nakamura, M. Kondo, et al. 2017. Guidance of regulatory T cell development by Satb1-dependent super-enhancer establishment. *Nat. Immunol.* 18:173–183. <https://doi.org/10.1038/ni.3646>
- Kometani, K., R. Nakagawa, R. Shinnakasu, T. Kaji, A. Rybouchkin, S. Moriyama, K. Furukawa, H. Koseki, T. Takemori, and T. Kurosaki. 2013. Repression of the transcription factor Bach2 contributes to predisposition of IgG1 memory B cells toward plasma cell differentiation. *Immunity*. 39:136–147. <https://doi.org/10.1016/j.jimmuni.2013.06.011>
- Kuwahara, M., W. Ise, M. Ochi, J. Suzuki, K. Kometani, S. Maruyama, M. Izumoto, A. Matsumoto, N. Takemori, A. Takemori, et al. 2016. Bach2-Batf interactions control Th2-type immune response by regulating the IL-4 amplification loop. *Nat. Commun.* 7:12596. <https://doi.org/10.1038/ncomms12596>
- Kuwahara, M., J. Suzuki, S. Tofukuji, T. Yamada, M. Kanoh, A. Matsumoto, S. Maruyama, K. Kometani, T. Kurosaki, O. Ohara, et al. 2014. The Menin-Bach2 axis is critical for regulating CD4 T-cell senescence and cytokine homeostasis. *Nat. Commun.* 5:3555. <https://doi.org/10.1038/ncomms4555>
- Levine, A.G., A. Arvey, W. Jin, and A.Y. Rudensky. 2014. Continuous requirement for the TCR in regulatory T cell function. *Nat. Immunol.* 15: 1070–1078. <https://doi.org/10.1038/ni.3004>
- Li, M.O., and A.Y. Rudensky. 2016. T cell receptor signalling in the control of regulatory T cell differentiation and function. *Nat. Rev. Immunol.* 16: 220–233. <https://doi.org/10.1038/nri.2016.26>
- Luche, H., O. Weber, T. Nageswara Rao, C. Blum, and H.J. Fehling. 2007. Faithful activation of an extra-bright red fluorescent protein in “knock-in” Cre-reporter mice ideally suited for lineage tracing studies. *Eur. J. Immunol.* 37:43–53. <https://doi.org/10.1002/eji.200636745>
- Luo, C.T., W. Liao, S. Dadi, A. Toure, and M.O. Li. 2016. Graded Foxo1 activity in Treg cells differentiates tumour immunity from spontaneous autoimmunity. *Nature*. 529:532–536. <https://doi.org/10.1038/nature16486>
- Miyara, M., Y. Yoshioka, A. Kitoh, T. Shima, K. Wing, A. Niwa, C. Parizot, C. Taflin, T. Heike, D. Valeyre, et al. 2009. Functional delineation and differentiation dynamics of human CD4+ T cells expressing the FoxP3 transcription factor. *Immunity*. 30:899–911. <https://doi.org/10.1016/j.jimmuni.2009.03.019>
- Orkin, S.H., and L.I. Zon. 2008. Hematopoiesis: an evolving paradigm for stem cell biology. *Cell*. 132:631–644. <https://doi.org/10.1016/j.cell.2008.01.025>
- Petersen, R.P., M.J. Campa, J. Sperlazza, D. Conlon, M.B. Joshi, D.H. Harpole, Jr., and E.F. Patz, Jr.. 2006. Tumor infiltrating Foxp3+ regulatory T-cells are associated with recurrence in pathologic stage I NSCLC patients. *Cancer*. 107:2866–2872. <https://doi.org/10.1002/cncr.22282>
- Pierson, W., B. Cauwe, A. Policheni, S.M. Schlenner, D. Franckaert, J. Berges, S. Humblet-Baron, S. Schönenfeldt, M.J. Herold, D. Hildeman, et al. 2013. Anti-apoptotic Mcl-1 is critical for the survival and niche-filling capacity of Foxp3+ regulatory T cells. *Nat. Immunol.* 14:959–965. <https://doi.org/10.1038/ni.2649>
- Quezada, S.A., K.S. Peggs, T.R. Simpson, and J.P. Allison. 2011. Shifting the equilibrium in cancer immunoediting: from tumor tolerance to eradication. *Immunol. Rev.* 241:104–118. <https://doi.org/10.1111/j.1600-065X.2011.01007.x>
- Roberts, A., H. Pimentel, C. Trapnell, and L. Pachter. 2011. Identification of novel transcripts in annotated genomes using RNA-Seq. *Bioinformatics*. 27:2325–2329. <https://doi.org/10.1093/bioinformatics/btr355>
- Roychoudhuri, R., D. Clever, P. Li, Y. Wakabayashi, K.M. Quinn, C.A. Klebanoff, Y. Ji, M. Sukumar, R.L. Eil, Z. Yu, et al. 2016a. BACH2 regulates CD8(+) T cell differentiation by controlling access of AP-1 factors to enhancers. *Nat. Immunol.* 17:851–860. <https://doi.org/10.1038/ni.3441>
- Roychoudhuri, R., R.L. Eil, D. Clever, C.A. Klebanoff, M. Sukumar, F.M. Grant, Z. Yu, G. Mehta, H. Liu, P. Jin, et al. 2016b. The transcription factor BACH2 promotes tumor immunosuppression. *J. Clin. Invest.* 126: 599–604. <https://doi.org/10.1172/JCI82884>
- Roychoudhuri, R., K. Hirahara, K. Mousavi, D. Clever, C.A. Klebanoff, M. Bonelli, G. Sciumè, H. Zare, G. Vahedi, B. Dema, et al. 2013. BACH2 represses effector programs to stabilize T(reg)-mediated immune homeostasis. *Nature*. 498:506–510. <https://doi.org/10.1038/nature12199>
- Rubtsov, Y.P., R.E. Nied, S. Josefowicz, L. Li, J. Darce, D. Mathis, C. Benoist, and A.Y. Rudensky. 2010. Stability of the regulatory T cell lineage in vivo. *Science*. 329:1667–1671. <https://doi.org/10.1126/science.1191996>
- Rubtsov, Y.P., J.P. Rasmussen, E.Y. Chi, J. Fontenot, L. Castelli, X. Ye, P. Treuting, L. Siewe, A. Roers, W.R. Henderson, Jr., et al. 2008. Regulatory T cell-derived interleukin-10 limits inflammation at environmental interfaces. *Immunity*. 28:546–558. <https://doi.org/10.1016/j.jimmuni.2008.02.017>
- Sakaguchi, S., T. Yamaguchi, T. Nomura, and M. Ono. 2008. Regulatory T cells and immune tolerance. *Cell*. 133:775–787. <https://doi.org/10.1016/j.cell.2008.05.009>
- Sebastian, M., M. Lopez-Ocasio, A. Metidji, S.A. Rieder, E.M. Shevach, and A.M. Thornton. 2016. Helios Controls a Limited Subset of Regulatory T Cell Functions. *J. Immunol.* 196:144–155. <https://doi.org/10.4049/jimmunol.1501704>
- Shankaran, V., H. Ikeda, A.T. Bruce, J.M. White, P.E. Swanson, L.J. Old, and R.D. Schreiber. 2001. IFNgamma and lymphocytes prevent primary tumour development and shape tumour immunogenicity. *Nature*. 410: 1107–1111. <https://doi.org/10.1038/35074122>
- Shinnakasu, R., T. Inoue, K. Kometani, S. Moriyama, Y. Adachi, M. Nakayama, Y. Takahashi, H. Fukuyama, T. Okada, and T. Kurosaki. 2016. Regulated selection of germinal-center cells into the memory B cell compartment. *Nat. Immunol.* 17:861–869. <https://doi.org/10.1038/ni.3460>
- Sidwell, T., Y. Liao, A.L. Garnham, A. Vasanthakumar, R. Gloury, J. Blume, P.P. Teh, D. Chisanga, C. Thelemann, F. de Labastida Rivera, et al. 2020. Attenuation of TCR-induced transcription by Bach2 controls regulatory T cell differentiation and homeostasis. *Nat. Commun.* 11:252. <https://doi.org/10.1038/s41467-019-14112-2>
- Smigiel, K.S., E. Richards, S. Srivastava, K.R. Thomas, J.C. Dudda, K.D. Klonowski, and D.J. Campbell. 2014. CCR7 provides localized access to IL-2 and defines homeostatically distinct regulatory T cell subsets. *J. Exp. Med.* 211:121–136. <https://doi.org/10.1084/jem.20131142>
- Stockis, J., R. Roychoudhuri, and T.Y.F. Halim. 2019. Regulation of regulatory T cells in cancer. *Immunology*. 157:219–231. <https://doi.org/10.1111/imm.13064>
- Subramanian, A., P. Tamayo, V.K. Mootha, S. Mukherjee, B.L. Ebert, M.A. Gillette, A. Paulovich, S.L. Pomeroy, T.R. Golub, E.S. Lander, et al. 2005. Gene set enrichment analysis: a knowledge-based approach for interpreting genome-wide expression profiles. *Proc. Natl. Acad. Sci. USA*. 102: 15545–15550. <https://doi.org/10.1073/pnas.0506580102>
- Tanaka, A., and S. Sakaguchi. 2017. Regulatory T cells in cancer immunotherapy. *Cell Res.* 27:109–118. <https://doi.org/10.1038/cr.2016.151>
- Turner, R., and R. Tjian. 1989. Leucine repeats and an adjacent DNA binding domain mediate the formation of functional cFos-cJun heterodimers. *Science*. 243:1689–1694. <https://doi.org/10.1126/science.2494701>
- Vahl, J.C., C. Drees, K. Heger, S. Heink, J.C. Fischer, J. Nedjic, N. Ohkura, H. Morikawa, H. Poeck, S. Schallenberg, et al. 2014. Continuous T cell receptor signals maintain a functional regulatory T cell pool. *Immunity*. 41:722–736. <https://doi.org/10.1016/j.jimmuni.2014.10.012>
- Wu, D., Q. Huang, P.C. Orban, and M.K. Levings. 2020. Ectopic germline recombination activity of the widely used Foxp3-YFP-Cre mouse: a case report. *Immunology*. 159:231–241. <https://doi.org/10.1111/imm.13153>
- Yadav, M., C. Louvet, D. Davini, J.M. Gardner, M. Martinez-Llordella, S. Bailey-Bucktrout, B.A. Anthony, F.M. Sverdrup, R. Head, D.J. Kuster, et al. 2012. Neuropilin-1 distinguishes natural and inducible regulatory T cells among regulatory T cell subsets in vivo. *J. Exp. Med.* 209: 1713–1722-S19. <https://doi.org/10.1084/jem.20120822>

Supplemental material

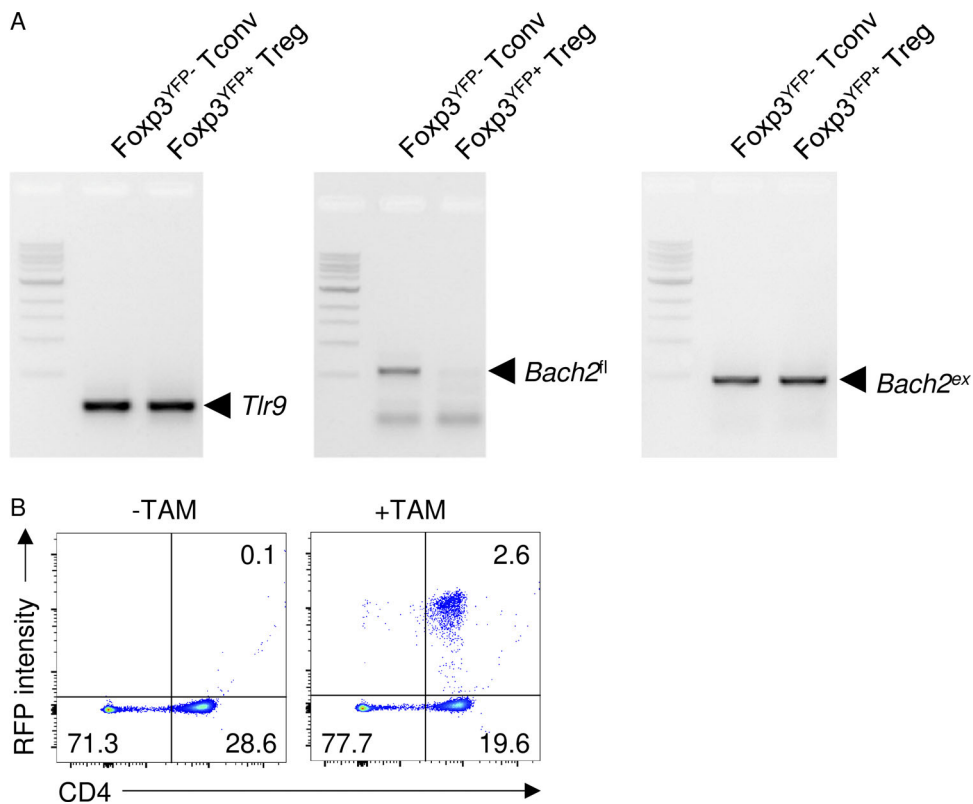


Figure S1. Assessment of nonspecific Cre activity in *Bach2^{fl/fl}* *Foxp3^{YFP-Cre}* mice. **(A)** Nonspecific deletion of the *Bach2^{fl}* allele in Tconv cells from *Bach2^{fl/fl}* *Foxp3^{YFP-Cre}* mice. PCR-based detection of the indicated alleles from *Foxp3⁻* Tconv cells and *Foxp3⁺* Treg cells isolated by FACS from *Bach2^{fl/fl}* *Foxp3^{YFP-Cre}* mice. Amplified fragments of control *Tlr9* (left), unexcised *Bach2^{fl}* (middle), or excised *Bach2^{ex}* alleles (right) are shown and indicated with black triangles. The *Bach2^{ex}* allele results from Cre-mediated excision of the *Bach2^{fl}* allele. The presence of detectable *Bach2^{ex}* amplicons from both Tconv and Treg cells indicates non-specific Cre-mediated excision of the *Bach2^{fl}* allele in Tconv cells, which is incomplete, as reflected by the presence of a residual *Bach2^{fl}* amplicon from Tconv cells. **(B)** Specific induction of RFP fluorescence within a fraction of CD4⁺ T cells upon tamoxifen treatment. Representative flow cytometry plot showing RFP intensity among CD4 T cells from spleens of *Bach2^{fl/fl}* *Foxp3^{EGFP-Cre-ERT2}* *Rosa26^{floxSTOP-tdRFP}* mice treated without (-TAM) or with (+TAM) tamoxifen in the diet for 8 wk. Data are representative of two repeated experiments with four mice per group. Numbers in gates show percentages. Bars and error show mean and SEM.

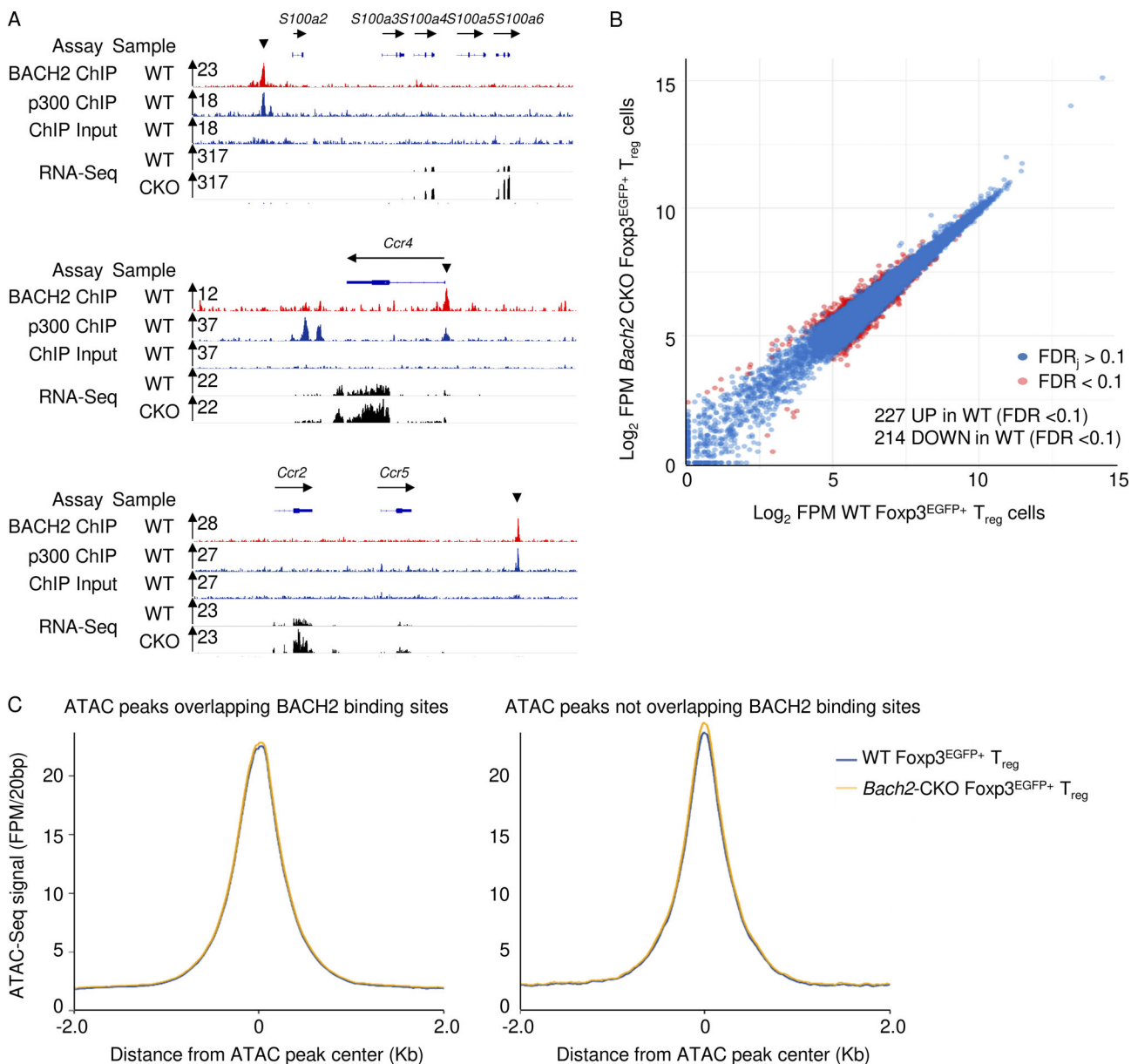


Figure S2. Genome-wide analysis of chromatin accessibility in WT and *Bach2*-deficient Treg cells. **(A)** Representative alignments of ChIP-Seq measurements showing binding of BACH2 and p300 at the indicated loci and RNA-Seq measurements from EGFP+ Treg cells from tamoxifen-treated *Bach2*^{+/+} *Foxp3*^{EGFP-Cre-ERT2} (WT) and *Bach2*^{fl/fl} *Foxp3*^{EGFP-Cre-ERT2} (CKO) animals. Representative alignments of RNA-Seq from three biological replicates per genotype are shown. **(B)** Differential analysis of global chromatin accessibility within *Foxp3*^{EGFP-Cre-ERT2} Treg cells from tamoxifen-treated *Bach2*^{+/+} *Foxp3*^{EGFP-Cre-ERT2} (WT) and *Bach2*^{fl/fl} *Foxp3*^{EGFP-Cre-ERT2} (CKO) animals. Mean ATAC-Seq signal at called ATAC-Seq peaks (peak calling threshold FDR < 0.05; binomial distribution) are shown as points. Significantly differentially accessible peaks between genotypes (FDR < 0.1; Wald test with Benjamini-Hochberg correction) are indicated as red points (227 peaks UP in WT and 214 peaks DOWN in WT; FDR < 0.1). **(C)** Histogram showing mean ATAC-Seq signal around called ATAC-Seq peak centers which either overlap (left) or do not overlap (right) BACH2 binding sites (peak calling threshold FDR < 0.05; binomial distribution). Data are representative of three ATAC-Seq and RNA-Seq replicates per genotype.

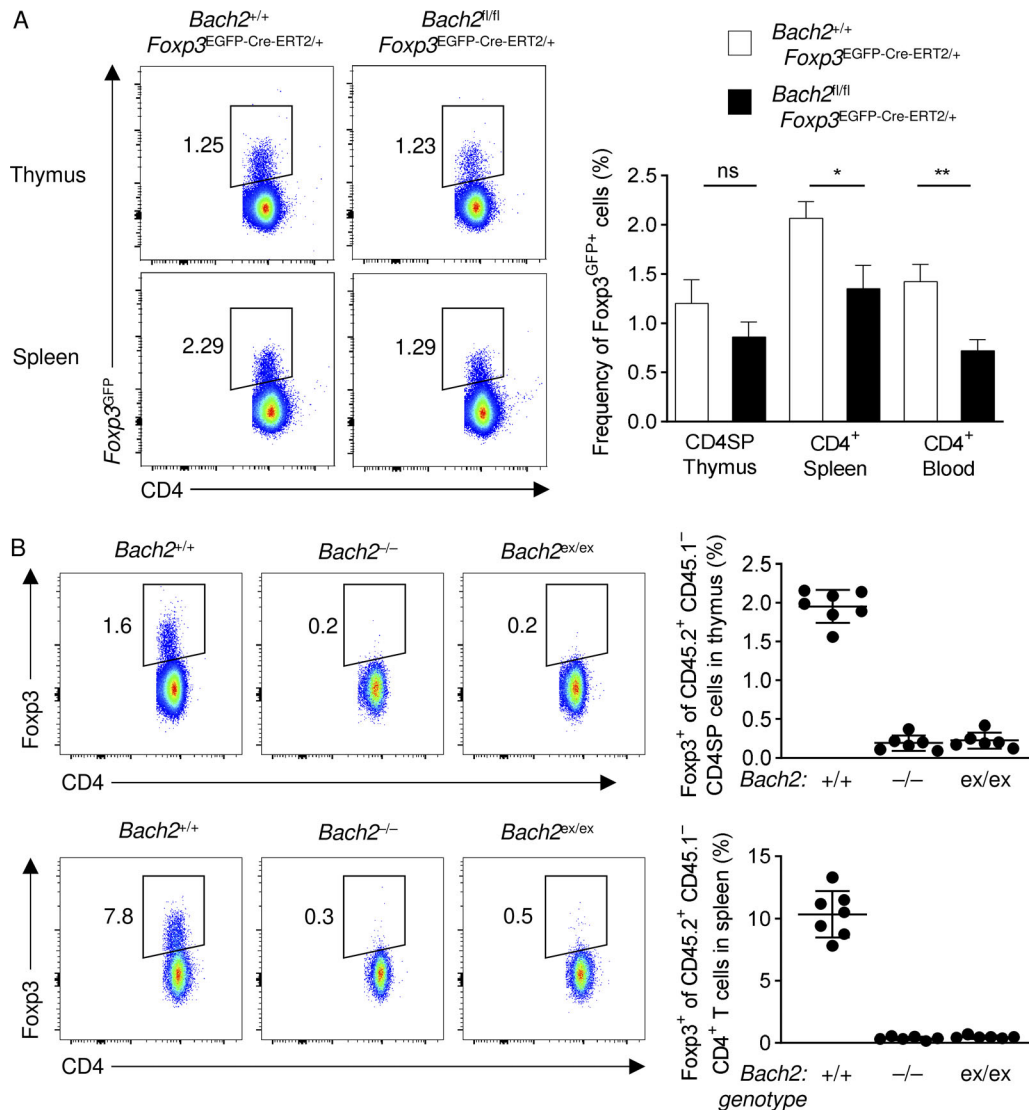


Figure S3. The phenotype of Foxp3⁺ Treg cells in *Bach2*^{fl/fl} *Foxp3*^{EGFP-Cre-ERT2/+} mice. **(A)** Representative flow cytometry (left) and the normalized percentage (right) of EGFP⁺ Treg cells from thymi (gated on CD4SP cells) or spleens (gated on CD4⁺ T cells) of animals of the indicated genotypes fed tamoxifen for 8 wk. **(B)** Homozygous germline excision of the *Bach2*^{fl} allele results in a complete cell-intrinsic defect in the generation of Foxp3⁺ Treg cells. Representative flow cytometry (left) and replicate measurements (right) showing the frequency of Foxp3⁺ Treg cells within the CD45.2⁺ compartment of CD45.1⁺ (*Ptprc*^{a/a}) mice reconstituted following lethal irradiation with mixtures of WT CD45.1/2⁺ (*Ptprc*^{a/b}) BM cells in an ~1:1 ratio with CD45.2⁺ BM cells from either *Bach2*^{+/+}, *Bach2*^{-/-}, or *Bach2*^{ex/ex} animals. A complete cell-intrinsic defect in generation of Foxp3⁺ cells is observed in either cells bearing the originally described *Bach2* knockout alleles (*Bach2*^{-/-}) or those with germline excision of *Bach2*^{flox} alleles, whereas Treg cells are produced by the WT (*Bach2*^{+/+}) BM compartments. Mice (*Bach2*^{ex/ex}) bearing germline excision of the *Bach2*^{flox} alleles were generated by transiently administering tamoxifen to male *Bach2*^{fl/fl} *Rosa26Cre-ERT2* mice which, after 2 mo, were used to breed with WT C57BL/6 female mice. F1 progeny bearing germline excision of the *Bach2*^{fl} allele were then backcrossed to generate *Bach2*^{ex/ex} animals, which were used to source cells for the BM chimera experiments described above. Data are representative of two independently repeated experiments with five (A) and six to seven (B) mice per group. *, P < 0.05; **, P < 0.01; ns, not significant; unpaired two-tailed Student's t test (A). Numbers in gates show percentages. Bars and error show mean and SEM.

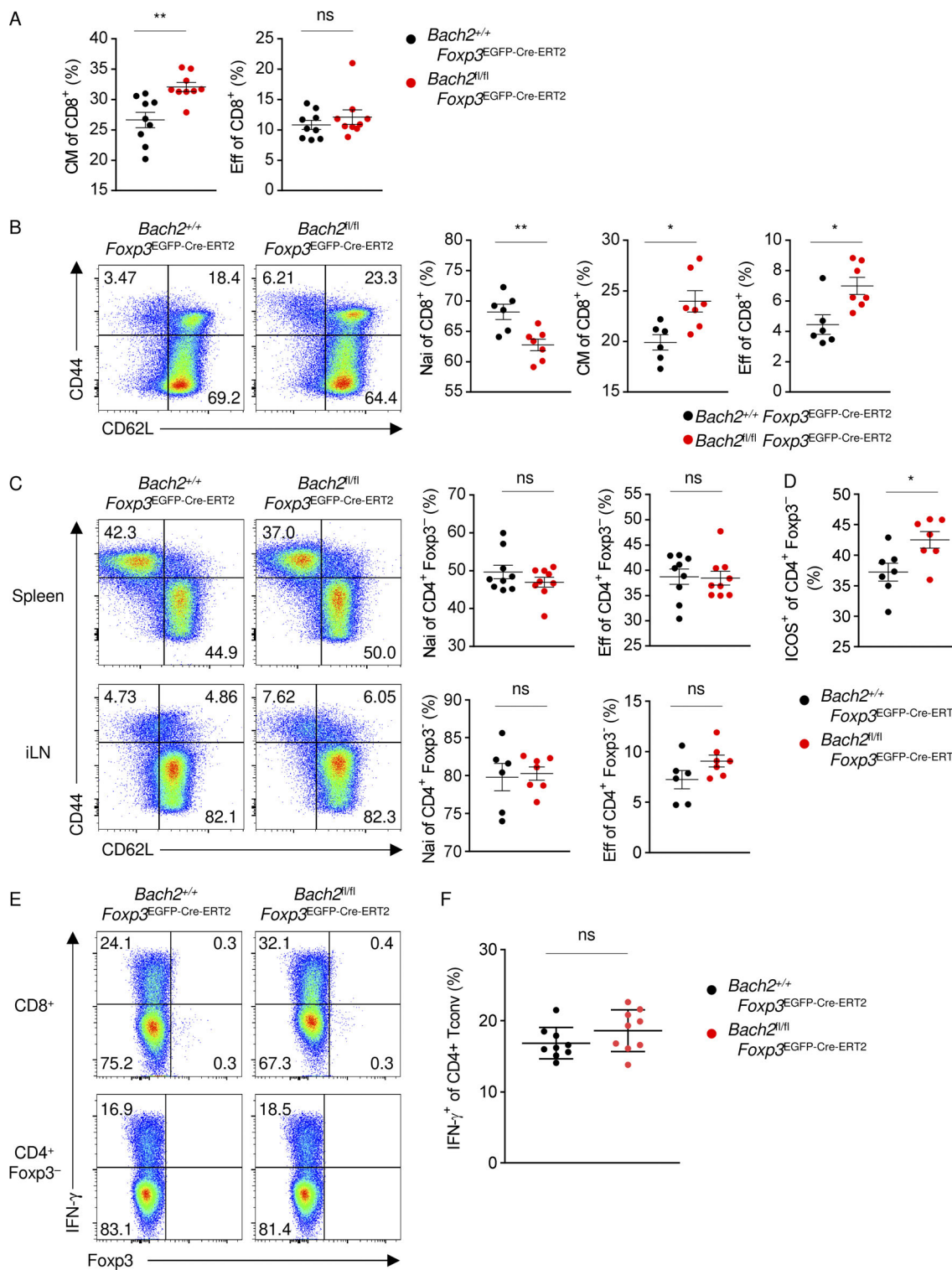


Figure S4. The phenotype of CD4⁺ and CD8⁺ Tconv cells in *Bach2*^{fl/fl} *Foxp3*^{EGFP-Cre-ERT2} mice. (A) Frequencies of indicated CD8⁺ T cell subsets within spleens of animals of the indicated genotypes treated with tamoxifen for 8 wk. (B) Representative flow cytometry showing CD44 and CD62L expression on gated CD8⁺ T cells (left) and frequencies of indicated T cell subsets (right) within inguinal lymph nodes of animals of the indicated genotypes treated with tamoxifen for 8 wk. (C) Representative flow cytometry showing CD44 and CD62L expression on gated CD4⁺ T cells (left) and frequencies of indicated T cell subsets (right) within spleens of animals of the indicated genotypes treated with tamoxifen for 8 wk. (D) Frequency of ICOS-expressing CD4⁺ T cells within spleens of animals of the indicated genotypes treated with tamoxifen for 8 wk. (E) Representative flow cytometry of IFN- γ expression by gated CD8⁺ and Foxp3⁻ CD4⁺ T cells from spleens of animals of the indicated genotypes treated with tamoxifen for 8 wk. (F) Frequency of IFN- γ -expressing CD4⁺ T cells from spleens of animals of the indicated genotypes treated with tamoxifen for 8 wk. Data are representative of two independently repeated experiments of nine (A), six to seven (B), six to nine (C), seven (D), and nine (E and F) mice per group. *, P < 0.05; **, P < 0.01; ns, not significant; unpaired two-tailed Student's t test (A–D and F). Numbers in gates show percentages. Bars and error show mean and SEM.

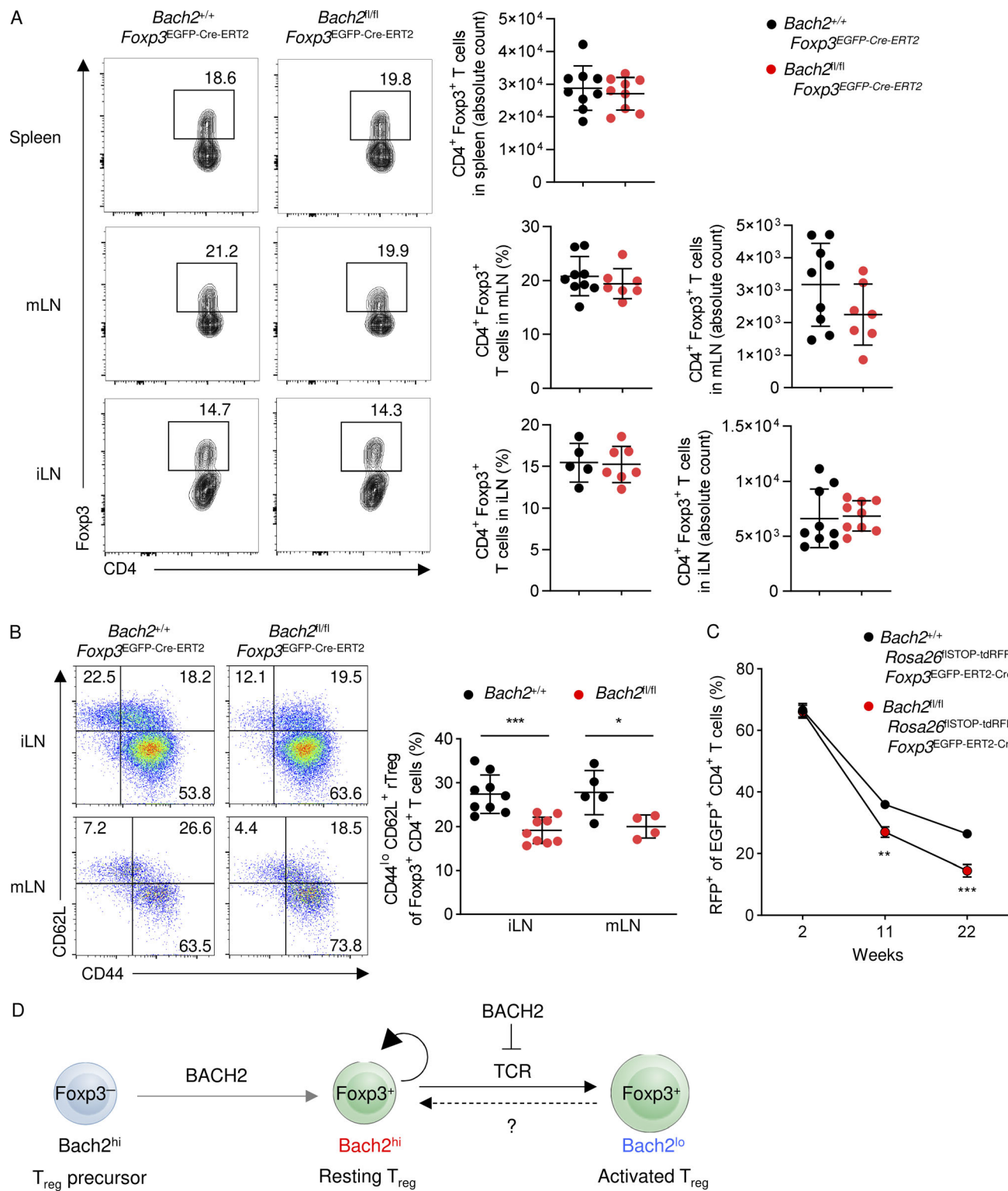


Figure S5. BACH2 after Treg lineage specification is required for long-term maintenance of Treg populations. **(A)** Representative flow cytometry (left) and replicate measurements (right) of Foxp3 expression among CD4⁺ T cells within indicated organs of tamoxifen-treated animals of the indicated genotypes. **(B)** Representative flow cytometry plots (left) and replicate measurements (right) of cell surface CD62L and CD44 expression by Treg cells isolated from the indicated lymphoid tissues from animals of the indicated genotypes fed tamoxifen for 8 wk. **(C)** Unnormalized frequency of RFP⁺ (pulse-labeled) cells within bulk Foxp3^{EGFP⁺} Treg cells in the blood of animals of the indicated genotypes at the indicated time points following the start of the pulse-labeling experiment. Data are representative of two independently repeated experiments. **(D)** Schematic representation of the functions of BACH2 before and after Treg lineage specification. *, P < 0.05; **, P < 0.01; ***, P < 0.001; unpaired two-tailed Student's t test (B and C). Numbers in gates show percentages. Data are representative of two independently repeated experiments of five to nine (A), four to nine (B) and five to seven (C) mice per group. Bars and error show mean and SEM.

Provided online are 16 tables. Table S1 shows genes up-regulated in *Bach2*^{tdRFP-low} versus *Bach2*^{tdRFP-high} Treg cells, purified from the spleens of *Foxp3*^{GFP-DTR} *Bach2*^{tdRFP/+} mice using FACS. Table S2 shows GSEA of global gene expression changes between *Foxp3*^{GFP}-positive *Bach2*^{tdRFP-low} Treg cells and *Foxp3*^{GFP}-positive *Bach2*^{tdRFP-high} Treg cells purified from the spleens of *Foxp3*^{GFP-DTR} *Bach2*^{tdRFP/+} mice using FACS. Table S3 lists the most significantly enriched hallmark gene sets in *Foxp3*^{GFP}-positive *Bach2*^{tdRFP-low} Treg cells versus *Foxp3*^{GFP}-positive *Bach2*^{tdRFP-high} Treg cells purified from the spleens of *Foxp3*^{GFP-DTR} *Bach2*^{tdRFP/+} mice using FACS. Table S4 shows GSEA of the HALLMARK_APOPTOSIS gene set within global gene expression differences between *Bach2*^{tdRFP-low} and *Bach2*^{tdRFP-high} Treg cells purified from the spleens of *Foxp3*^{GFP-DTR} *Bach2*^{tdRFP/+} mice using FACS. Table S5 shows scRNA-Seq frequency (percentage positive) of single cells expressing within each cluster after downsampling for sequencing depth and normalized to cell number per sample. Table S6 shows scRNA-Seq genes exhibiting significant differential enrichment between clusters. Table S7 lists genes up-regulated in cluster 0 versus cluster 4 from TSNE analysis of single *Foxp3*^{EGFP}-positive Treg cells. Table S8 lists differentially expressed genes between WT and *Bach2*-deficient cluster 0 Treg cells ($P_{ADJ} < 0.05$). Table S9 lists differentially expressed genes between WT and *Bach2*-deficient cluster 4 Treg cells ($P_{ADJ} < 0.05$). Table S10 shows GSEA of genes significantly up-regulated in *Bach2*^{tdRFP-low} versus *Bach2*^{tdRFP-high} Treg cells within the global transcriptional differences between *Foxp3*^{EGFP}-positive Treg cells from tamoxifen-treated *Bach2*^{FL/FL} *Foxp3*^{EGFP-CRE-ERT2} versus *Bach2*^{+/+} *Foxp3*^{EGFP-CRE-ERT2} animals measured by bulk RNA sequencing. Table S11 shows the genomic locations of significantly enriched BACH2 binding sites identified by ChIP-Seq within iTreg cells. Table S12 shows gene expression in *Foxp3*^{EGFP}-positive Treg cells purified by FACS from *Bach2*^{FL/FL} *Foxp3*^{EGFP-CRE-ERT2} and *Bach2*^{+/+} *Foxp3*^{EGFP-CRE-ERT2} animals treated with tamoxifen. Table S13 shows genome-wide analysis of differentially accessible chromatin in *Bach2*^{+/+} *Foxp3*^{EGFP-CRE-ERT2} (WT) and *Bach2*^{FL/FL} *Foxp3*^{EGFP-CRE-ERT2} (CKO) animals. Table S14 lists the genomic locations of significantly enriched JunD binding sites identified by ChIP-Seq within iTreg cells. Table S15 shows colocalized genomic binding sites between BACH2 and JunD within in vitro-generated iTreg cells. Table S16 lists fluorochrome-conjugated antibodies used in the study.